

1 **Variations and sources of volatile organic compounds (VOCs)**
2 **in urban region: insights from measurements on a tall tower**

3 Xiao-Bing Li^{1,2}, Bin Yuan^{1,2,*}, Sihang Wang^{1,2}, Chunlin Wang^{3,4}, Jing Lan^{3,4}, Zhijie
4 Liu^{1,2}, Yongxin Song^{1,2}, Xianjun He^{1,2}, Yibo Huangfu^{1,2}, Chenglei Pei^{5,6,7,8}, Peng
5 Cheng⁹, Suxia Yang^{1,2}, Jipeng Qi^{1,2}, Caihong Wu^{1,2}, Shan Huang^{1,2}, Yingchang You^{1,2},
6 Ming Chang^{1,2}, Huadan Zheng¹⁰, Wenda Yang⁹, Xuemei Wang^{1,2}, and Min Shao^{1,2}

7 ¹ Institute for Environmental and Climate Research, Jinan University, Guangzhou
8 511443, China

9 ² Guangdong-Hongkong-Macau Joint Laboratory of Collaborative Innovation for
10 Environmental Quality, Guangzhou 511443, China

11 ³ Guangzhou Climate and Agrometeorology Center, Guangzhou, 511430, China

12 ⁴ Southern Marine Science and Engineering Guangdong Laboratory (Zhuhai), Zhuhai,
13 519082, China

14 ⁵ State Key Laboratory of Organic Geochemistry and Guangdong Key Laboratory of
15 Environmental Protection and Resources Utilization, Guangzhou Institute of
16 Geochemistry, Chinese Academy of Sciences, Guangzhou 510640, China

17 ⁶ CAS Center for Excellence in Deep Earth Science, Guangzhou, 510640, China

18 ⁷ University of Chinese Academy of Sciences, Beijing 100049, China

19 ⁸ Guangzhou Ecological and Environmental Monitoring Center of Guangdong Province,
20 Guangzhou 510060, China

21 ⁹ Institute of Mass Spectrometer and Atmospheric Environment, Jinan University,
22 Guangzhou 510632, Guangdong, China

23 ¹⁰ Guangdong Provincial Key Laboratory of Optical Fiber Sensing and
24 Communications, and Department of Optoelectronic Engineering, Jinan University,
25 Guangzhou, 510632, China

26 * Corresponding authors: byuan@jnu.edu.cn

27 Abstract

28 Volatile organic compounds (VOCs) are key precursors of ozone and particulate
29 matter, ~~that~~ which are the two dominant air pollutants in urban environments. However,
30 compositions and sources of VOCs in urban air aloft were rarely reported ~~by~~ so far. To
31 address this matter, highly time-resolved measurements of VOCs were made by proton-
32 transfer-reaction time-of-flight mass spectrometer (PTR-ToF-MS) at a 450-m platform
33 on the Canton Tower in Guangzhou, China. A combination of *in-situ* measurements and
34 modeling techniques was used to characterize variations and sources of VOCs. Five
35 sources were identified from positive matrix factorization (PMF) analysis, namely
36 daytime-mixed (e.g., biogenic emissions and secondary formation), visitor-related (e.g.,
37 human breath, cooking, and volatilization of ethanol-containing products),
38 vehicular+industrial, regional transport, and volatile chemical product (VCP)-
39 dominated (i.e., volatilization of personal care products), contributing on average to
40 ~~222~~ 21%, 30%, 28%, 10%, and 11% of total VOCs (TVOC) mixing ratios, respectively.
41 We observe that contributions of the visitor-related source, mainly composed of ethanol,
42 followed well with the variation ~~patterns of~~ in visitor numbers on the tower. The VCP-
43 dominated source only had an average contribution of ~5.7 ppb during the campaign,
44 accounting for a small fraction (11%) of TVOC mixing ratios but a large fraction (22%)
45 of the total OH reactivity. However, large fractions of ~~some~~ reactive VOC species, e.g.,
46 monoterpenes (49%), were attributed to the VCP-dominated source, indicating
47 significant important contributions of VCPs to ambient concentrations of these species
48 in urban environments. Vertical profiles of air pollutants (including namely NO_x, ozone,
49 O_x, and PM_{2.5}), measured at 5 m, 118 m, 168 m, and 488 m, exhibited more evident
50 gradients at night than in the daytime owing to the stronger stability of the nocturnal
51 boundary layer. Mixing ratios of VOC species during the nighttime generally decreased
52 with time when the 450-m platform was located in the nocturnal residual layer and
53 significantly markedly increased when impacted by emissions at ground. The results in

54 this study demonstrated composition characteristics and sources of VOCs in urban air
55 aloft, which could provide valuable implications in making control strategies of VOCs
56 and secondary air pollutants.

57 1 Introduction

58 Volatile organic compounds (VOCs) are important trace gases in the atmosphere
59 and are composed of myriad chemical species (Pallavi et al., 2019; Wang et al., 2020a;
60 Gkatzelis et al., 2021). Except for their direct adverse impacts on human health (Zhang
61 et al., 2013), VOCs are also ~~contributed significantly to the formation~~important
62 precursors of secondary pollutants such as ozone and secondary aerosol (Vo et al., 2018;
63 Zhou et al., 2019; Qin et al., 2021). Reduction in ambient VOCs concentrations is the
64 key for synergistic control of both ozone and particle pollution. However, it is highly
65 challenging for this target due to complex sources and chemical transformations of
66 VOCs in urban environments (Yuan et al., 2012; Mo et al., 2016; Zhu et al., 2019).

67 In addition to compiling accurate emission inventories (bottom-up method)
68 (Zheng et al., 2013; An et al., 2021), the combination of *in-situ* measurements and
69 receptor models (top-down method) was widely adopted to quantitatively apportion
70 sources of ambient VOCs (Baudic et al., 2016; Liu et al., 2016; Fan et al., 2021; Pernov
71 et al., 2021). Concentrations of various VOC species ~~could~~can be measured by offline
72 and online techniques. Gas chromatography-flame ionization detector/mass
73 spectrometry (GC-FID/MS) combined with stainless steel canisters ~~were~~are the most
74 popular offline technique ~~for VOCs measurements~~ (Guo et al., 2011; Yuan et al., 2013;
75 Zhang et al., 2013; Qin et al., 2021). Automated online GC-FID system and high time
76 resolution mass spectrometer, such as proton-transfer-reaction mass spectrometer
77 (PTR-MS) and chemical ionization mass spectrometer (CIMS), ~~were~~are popular online
78 techniques ~~for VOCs measurements~~ (de Gouw and Warneke, 2007; Wang et al., 2020a;
79 Wang et al., 2020c; Fan et al., 2021; Ye et al., 2021). However, VOCs measurements
80 made by both online and offline instruments are ~~significantly~~markedly affected by very
81 local emission sources, particularly in urban environments, when they are usually
82 deployed at ground level. This is highly important for studies aiming to characterize
83 variations and sources of ambient VOCs at large spatial scales (such as a city or city

84 clusters) based on measurements of only one site. To address this concern, VOCs
85 measurements made in the upper part of the planetary boundary layer (PBL) may be a
86 better choice due to the well mixing of surface emissions when being transported
87 upward from sources to observation sites (Hu et al., 2015a; Hu et al., 2015b; Squires et
88 al., 2020).

89 As reported in the literature, *in-situ* measurements of VOCs at high altitudes (e.g.,
90 hundreds of meters or several kilometers above ground level) were predominantly made
91 using the combination of offline techniques and samples collected by various platforms
92 such as aircrafts (Geng et al., 2009; Xue et al., 2011; Benish et al., 2020), tethered
93 balloons (Zhang et al., 2018; Wu et al., 2020b; Wang et al., 2021; Wu et al., 2021), high
94 buildings and towers (Ting et al., 2008; Mo et al., 2020), and unmanned aerial vehicles
95 (UAVs) (Vo et al., 2018; Liu et al., 2021). These offline measurements were
96 predominantly used to reveal vertical variations of VOCs concentrations, impacts of
97 VOCs degradation chemistry on the formation of secondary pollutants, and source
98 characteristics of the species of interest. Offline measurements made at high altitudes
99 were generally not capable of fully characterizing temporal variations of concentrations
100 and source characteristics of VOCs due to strict limitations in their time resolution and
101 sample sizes. In this condition, online VOCs measurements with fast response at high
102 altitudes are required. Lack of available platforms has been a key limited factor for
103 conducting online VOCs measurements at high altitudes in China. For instance, the
104 combined utilization of aircraft and online spectrometer (such as PTR-MS) has been
105 widely used in North America to measure VOCs concentrations in the lower
106 troposphere (Hornbrook et al., 2011; Müller et al., 2016; Yuan et al., 2016; Koss et al.,
107 2017; Fry et al., 2018; Chen et al., 2019), while it is quite difficult in China due to the
108 lack of professional research aircraft and the strict control of airspace. Tethered balloons
109 and UAVs are generally not suitable for online VOCs measurements due to their limited
110 payloads (Dieu Hien et al., 2019). Tower-based platforms provide another path for
111 online VOCs measurements at high altitudes in urban environments. However, tower-

112 based online measurements of VOCs were only reported in Beijing, China ~~by so~~ far
113 (Squires et al., 2020; Zhang et al., 2020).

114 In this study, continuous online VOCs measurements, including more than 200
115 ~~chemical~~ species with a time resolution of 10 s, were made at a 450-m platform on the
116 Canton Tower in the Pearl River Delta (PRD) region, China during August–November
117 2020. A combination of the VOCs measurements and the positive matrix factorization
118 (PMF) receptor model was used to provide new insights into the concentrations,
119 temporal variations, and source contributions of VOCs in urban region.

120 **2 Methods and materials**

121 **2.1 Site description and field campaign**

122 The PRD region is one of the most developed city clusters in China with more
123 than 70 million residents by 2020 and is suffering from air pollution problems (e.g.,
124 ozone and secondary aerosol) (Wang et al., 2017; Wang et al., 2020b; Yan et al., 2020;
125 Li et al., 2022). In this study, VOCs measurements were made at the Canton Tower
126 (CTT, 23.11°N, 113.33°E) in Guangzhou, a large city in PRD (Figure S1), from August
127 18 to November 5 in 2020. The CTT has a total height of 610 m including the shaft on
128 the top ([Figure S1\(c\)](#)). The observation was conducted in a room (Figure S1) at the 450-
129 m Look Out platform ([Jin et al., 2022](#)), which is a ramp with stairs and is located on the
130 top of the main body of the CTT. The observation room is located below the ramp and
131 a sampling port is reserved on the wall outside the tower. ~~has a~~ louver is located ~3
132 m below the sampling port. The 450-m Look Out platform is a famous tourist attraction
133 with an opening time of local time (LT, UTC+8) 10:00–22:30, and visitors could walk
134 around for a panorama of downtown Guangzhou. On each day, there are two busiest
135 tourist hours, roughly at LT 11:00–14:00 and 18:00–21:00, on the 450-m platform. In
136 addition, there are three restaurants between 376 and 423 m. The VOCs measurements
137 were interrupted during October 8–12 due to instrument malfunction.

138 2.2 VOCs measurements

139 VOCs measurements were made using a high-resolution proton-transfer-reaction
140 quadrupole interface time-of-flight mass spectrometer (PTR-QiToF-MS, Ionicon
141 Analytik, Innsbruck, Austria) with both hydronium ion (H_3O^+) (Yuan et al., 2017; Wu
142 et al., 2020a) and nitric oxide ion (NO^+) chemistry (Wang et al., 2020a). The H_3O^+ and
143 NO^+ modes were automatically switched with 22 min for the H_3O^+ mode and 12 min
144 for the NO^+ mode during the campaign. In this study, only VOCs measurements made
145 in the H_3O^+ mode were used for analysis. In H_3O^+ mode, the PTR-QiToF-MS was
146 operated with a drift tube pressure of 3.8 mbar, a drift tube temperature of 120 °C, and
147 a drift tube voltage of 760 V, resulting in an E/N (E refers to electric field and N refers
148 to number density of buffer gas in the drift tube) value of ~120 Td (Townsend). Raw
149 data of PTR-ToF-MS were processed and analyzed using Tofware software (Tofwerk
150 AG, v3.0.3) and please refer to our previous works (Wang et al., 2020a; Wu et al., 2020a)
151 for more details. Signals of 3035 ions with m/z up to 510 were obtained at time
152 resolutions of 10 s. To measure VOCs concentrations outside the tower, The sampling
153 inlet of the instrument was extended to the outside wall of the observation room using
154 a ~5-m long Perfluoroalkoxy (PFA) Teflon tubing (OD: 1/4") was used to connect the
155 inlet of the instrument and a reserved the sampling port on the wall of the observation
156 room (Figure S1). The PFA Teflon tubing has been proven to be effective in measuring
157 ambient concentrations of VOCs (Deming et al., 2019; Liu et al., 2019) and has been
158 widely used in field studies (de Gouw et al., 2003a; Hu et al., 2011; Wu et al., 2020a),
159 which Air sample is in the tubing was drawn by a pump at a flow rate of $\sim 5 \text{ L min}^{-1}$.
160 Blank measurements were performed automatically at the last 2 min of the H_3O^+ mode
161 by passing ambient air through a platinum catalyst heated to 365 °C. ~~Mass spectra of~~
162 ~~up to $m/z = 510$ were obtained at a time resolution of 10 s.~~

163 A gas standard with 35 VOC species (Table S1) was used for calibrations of the
164 PTR-ToF-MS once per day. Ten organic acids and nitrogen-containing VOC species
165 were calibrated using a liquid calibration unit in the laboratory (Table S1). Sensitivities

166 of the remaining VOC species were determined using the quantification method based
167 on reaction kinetics of the PTR-ToF-MS (Wu et al., 2020a; He et al., 2022). Impacts of
168 the change in ambient humidity on measured signals of the PTR-ToF-MS were removed
169 using humidity-dependence curves of VOC species determined in the laboratory (Wang
170 et al., 2020a; Wu et al., 2020a). The limit of detection (LOD) for a VOC species was
171 defined as the concentration when the signal-to-noise ratio (SNR) equals to 3 (Yuan et
172 al., 2017). Average mixing ratios, LODs, sensitivities, chemical formula, and suggested
173 compounds of 225 VOC species used in this study are summarized in Table S1.

174 2.3 Other measurements

175 During the CTT campaign, a CO₂ and H₂O Gas Analyzer (Model: Li-840A, Licor
176 Inc., USA) was deployed to measure carbon dioxide (CO₂, ppm in dry air) and humidity
177 (mmol mol⁻¹). In addition, four air quality automatic monitoring stations are located at
178 ground level (~5 m), 118 m, 168 m, and 488 m of the ~~tower~~CTT, which report hourly
179 concentrations of O₃ozone, NO, NO₂, NO_x, and PM_{2.5} along with meteorological
180 parameters, including namely temperature (T), relative humidity (RH), and pressure
181 (Mo et al., 2020). Mass concentrations of gaseous pollutants were reported at 25 °C and
182 1013.25 hPa and were converted to mixing ratios (ppb) accordingly. Contour plots of
183 vertical profiles of NO_x, ozone, Ox (O₃+NO₂), and PM_{2.5} concentrations were made
184 using the bilinear method in Igor software (v8.04). Linear interpolations for
185 concentrations of these pollutants were performed on both spatial (altitude) and
186 temporal scales. A ceilometer (CL31, Vaisala, Finland) deployed on the Panyu Campus
187 of Jinan University (23.02°N, 113.41°E, Figure S1), approximately 13.5 km to the
188 southeast of the CTT, was used to measure planetary boundary layer height (PBLH)
189 during the campaign. In addition, measurements of VOCs and CO₂ made on the campus
190 of Guangzhou Institute of Geochemistry (GIG), Chinese Academy of Sciences
191 (23.15°N, 113.36°E, ~25 m above ground level) during September–November 2018
192 (Wang et al., 2020a; Wang et al., 2020c; Wu et al., 2020a) were used for comparison
193 with those measured on the CTT. p values were obtained using the Student's t-test to

194 determine statistical significance levels of differences. The GIG site is located
195 approximately 5.7 km to the northeast of the CTT. Measurements of VOCs and CO₂ at
196 the GIG site were made using the same instruments as those at the CTT site.

197 **2.4 PMF receptor model**

198 The PMF receptor model was used to quantitatively analyze sources of the VOCs
199 measurements made at the 450-m platform. The PMF model has been widely used to
200 determine source contributions of measured VOCs concentrations in previous studies
201 (Yuan et al., 2012; Pallavi et al., 2019; Pernov et al., 2021). A simple description of the
202 PMF model was provided in the Supplementary Information (SI).

203 The PMF model was performed on 225 VOC species (Table S1) in this study
204 (~~Table S1~~). In preparation of PMF input data, measured concentrations of a VOC
205 species below the LOD were replaced with half of the LOD and corresponding
206 uncertainties were assigned to 5/6 of the LOD. Missing samples of a VOC species were
207 replaced with its median value during the campaign and corresponding uncertainties
208 were set as values equal to three times the median value (Zhang et al., 2013; Pernov et
209 al., 2021; Qin et al., 2021). In this studyDuring the CTT campaign, the measured
210 ethanol concentrations ~~on the 450-m platform~~ were ~~significantly~~ impacted by the
211 change in the number of visitors (a detailed discussion in Section 3.3) and exhibited
212 strong variations ~~during the campaign~~ (Figure 1). Thus, measurement uncertainties of
213 ethanol calculated by Eq. (S3) were reduced by a factor of 5 to increase ~~the its~~ weight
214 ~~of ethanol~~ in PMF analysis, which successfully resolved factors representing visitor
215 influences and ~~significantly~~ reduce residuals of PMF solution from over 20% to ~14%.
216 The PMF analysis was performed using the PMF Evaluation Tool (v3.05) with Igor Pro
217 (Ulbrich et al., 2009).

218 3 Results and discussion

219 3.1 Overview of field measurements during the campaign

220 As shown in Figure 1, concentrations of various species and meteorological
221 parameters all exhibited strong variations during the campaign. Daily mean ozone
222 mixing ratios varied in the range of 17.8–105.0 ppb with an average (\pm standard
223 deviation) of 55.1 ± 18.3 ppb. Daily mean total VOCs (TVOC) mixing ratios, including
224 a total of 225 species, varied between 23.9–124.2 ppb with an average of 62.1 ± 21.8
225 ppb. Daily mean NO_x mixing ratios varied in the range of 7.9–31.6 ppb with an average
226 of 13.6 ± 3.8 ppb. Measured CO₂ mixing ratios exhibited strong variability with daily
227 mean values ranging from 403.5 to 471.4 ppm. Ethanol was the most abundant VOC
228 species, accounting on average for 23.5% of measured TVOC mixing ratios ~~during the~~
229 ~~campaign~~. Daily mean ethanol mixing ratios varied between 4.3–53.4 ppb with an
230 average of 15.3 ± 9.1 ppb. Toluene was the most abundant aromatic species and had an
231 average mixing ratio of 1.4 ± 0.9 ppb ~~during the campaign~~. Daily mean temperatures
232 varied in the range of 17.7–29.0 °C with an average of 23.2 ± 3.0 °C. Daily mean RH
233 varied between 39.3%–85.0% with an average of $71.6\% \pm 10.3\%$. In general, the
234 observation site was predominantly influenced by hot and moist air masses from August
235 18 to October 4, but cooler and dryer air masses from October 5 to November 5.

236 The most abundant 10 VOC species measured by PTR-ToF-MS during the CTT
237 campaign were ethanol, methanol, acetic acid, formaldehyde, acetone, ethyl acetate,
238 acetaldehyde, hydroxyacetone+propionic acid, toluene, and C₈ aromatics, contributing
239 to over 70% of TVOC mixing ratios. As shown in Figure 2, the 225 VOC species were
240 classified into six categories, namely C_xH_y (i.e., hydrocarbons), C_xH_yO₁ (i.e., VOC
241 species containing one oxygen atom), C_xH_yO₂ (i.e., VOC species containing two
242 oxygen atoms), C_xH_yO_{≥3} (i.e., VOC species containing ~~more than three~~ or more oxygen
243 atoms), N/S containing species (i.e., VOC species containing nitrogen or sulfur atoms),
244 and siloxanes (Wu et al., 2020a; He et al., 2022). The most abundant category was

245 C_xH_yO₁, which had an average contribution of 62.267% to ~~measured~~-TVOC mixing
246 ratios, but only contributed to 40% of total OH reactivity. The C_xH_yO₂ and C_xH_yO_{≥3}
247 categories contributed to 24.92% and 2.91% of ~~measured~~-TVOC mixing ratios,
248 respectively. C_xH_y ~~was the third abundant category, only accounting~~ accounted for 6.49%
249 of ~~measured~~-TVOC mixing ratios but contributed to 37% of the total OH reactivity,
250 indicating more reactive VOC species in this category. Concentrations of N/S
251 containing species and siloxanes were generally lower than 0.5 ppb and ~~only totally~~
252 contributed to 1.3% and 2.4~1% of ~~measured~~-TVOC mixing ratios, ~~respectively~~.

253 At ground level, each VOCs category accounted for comparable fractions in
254 TVOC mixing ratios and the total OH reactivity to those measured at 450 m.
255 ~~However~~ As shown in Figure 2, the majority of the C_xH_y, C_xH_yO_{>3}C_xH_yO₃, and N/S
256 containing species measured at 450 m (~~CTT campaign~~) had lower mixing ratios than
257 those measured at ground level (~~GIG campaign~~) (Figures 2(b) and S2), indicating
258 implying their predominant contributions from surface emission sources. Most of the
259 C_xH_yO₁ and C_xH_yO₂ species measured at 450 m had comparable mixing ratios to those
260 measured at the ground level. However, mixing ratios of some C_xH_yO₂,
261 C_xH_yO_{>3}C_xH_yO₃, and N/S containing species measured at 450 m were significantly
262 higher than those measured at ~~the~~-ground level, which can be attributable to either
263 enhancement of their emissions on the 450-m platform or more secondary formation
264 from oxidation of VOCs (e.g., C_xH_y and C_xH_yO₁ species). The differences in
265 contributions of VOCs categories to the total concentrations and OH reactivity imply
266 that sources of the VOCs measurements made at 450 m and the ground level are
267 different.

268 3.2 Diurnal variations in selected VOC species

269 Average diurnal profiles of nine selected VOC species measured by PTR-ToF-MS
270 during the CTT campaign are demonstrated in Figure 3. Measurement results at GIG in
271 2018 are also shown for comparison to investigate differences in their diurnal variation
272 patterns and likely sources ~~when measured at ground level and in urban upper air~~. In

273 addition, average diurnal profiles of the selected VOC species on working and non-
274 working days (including weekends and public holidays when the 450-m platform had
275 more visitors) during the CTT campaign are compared to explore potential emissions
276 from visitors. Average diurnal variations in ratios of concentrations of selected VOC
277 species measured on non-working days to those measured on working days were also
278 calculated, as shown in Figure S3. Meteorological factors, ~~including namely~~
279 temperature and RH₂ exhibited insignificant differences between working and non-
280 working days (Figure S2S4). Thus, the differences of in VOCs concentrations between
281 working and non-working days for various species were not caused notably impacted
282 by the change in meteorological conditions.

283 Diurnal profiles of aromatic species, including benzene, toluene, and C8 aromatics
284 measured at 450 m exhibited similar variability with minima occurring between LT
285 12:00–16:00. Aromatics with higher chemical reactivity could be removed more rapidly
286 by reactions with hydroxyl radicals (OH) in the daytime (Yuan et al., 2012; Wu et al.,
287 2020a). In addition, ~~significant rapid~~ elevation of the daytime PBL could enhance the
288 dilution of chemical species, leading to rapid decreases in their concentrations
289 (Sangiorgi et al., 2011; Zhang et al., 2018). The two effects are the two most important
290 factors for controlling diurnal profiles of aromatics measured at 450 m. By contrast,
291 diurnal profiles of aromatics measured at ground displayed a different pattern with two
292 peaks occurring in the morning (LT 07:00–08:00) and evening (LT 19:00–22:00),
293 respectively. Diurnal patterns of aromatics are ~~highly~~ consistent with that of NO_x (a
294 typical tracer of traffic emissions in urban region) at ~~the~~ ground level but were
295 ~~significantly~~ different from that of NO_x at 450 m (Figure 4). Therefore, measured
296 concentrations of aromatics, particularly for benzene, were ~~significantly markedly~~
297 affected by traffic emissions at ground level, but contributed by more complex sources
298 at 450 m. The differences in diurnal profiles of aromatics ~~on between~~ working and non-
299 working days ~~exhibited minor were insignificant (p>0.05) differences,~~ implying
300 ~~insignificant minor~~ contributions from visitor-related emissions. On working days,

301 toluene concentrations measured at 450 m were more affected by traffic emissions as
302 manifested by the two ~~significant-remarkable~~ peaks in the morning and late afternoon.

303 Isoprene and monoterpenes exhibited distinct diurnal variation patterns during the
304 two campaigns. As reported in (Gómez et al., 2020; Tan et al., 2021), diurnal profiles
305 of isoprene and monoterpenes concentrations in non-urban regions usually displayed
306 unimodal patterns with a peak occurring at noon due to the strong light/temperature-
307 dependence of biogenic emissions. In this study, isoprene concentrations at 450 m
308 plateaued during the daytime and were slightly higher on non-working days than those
309 on working days, implying ~~significant-large~~ contributions from visitor-related
310 emissions. The diurnal profile of monoterpenes measured at 450 m exhibited a bi-modal
311 pattern with two peaks at LT 14:00 and 20:00, which was roughly in accordance with
312 diurnal peaks of visitor numbers on the 450-m platform. In addition, monoterpenes
313 concentrations at 450 m were significantly ($p<0.01$) higher on non-working days
314 (particularly during the busiest tourist hours) than on working days, confirming
315 significant contributions from visitor-related or cooking emissions (Klein et al., 2016).
316 The diurnal profiles of methyl vinyl ketone (MVK) + methacrolein (MACR)
317 demonstrated similar shapes to ozone at both 450 m and ground level with maxima
318 occurring between LT 13:00–15:00 (Figure 4), consistent with MVK+MACR as
319 photooxidation products of isoprene (Greenberg et al., 1999; Zhao et al., 2021). The
320 concentrations of MVK+MACR during the daytime on non-working days were also
321 ~~evidently-significantly~~ ($p<0.01$) higher than those on working days, which are
322 consistent with isoprene observations.

323 Acetone, methanol, and ethanol are abundant OVOC species in urban atmosphere.
324 Diurnal profiles of acetone measured at both 450 m and the ground level were
325 characterized by higher concentrations in the daytime, suggesting ~~significant~~
326 ~~predominant~~ contributions from daytime sources, such as vegetation emissions and
327 photooxidation of hydrocarbons (Hu et al., 2013; Gkatzelis et al., 2021). In addition,
328 acetone concentrations at 450 m were higher on non-working days than on working

329 days, implying prominent contributions from visitor-related emissions. Diurnal profiles
330 of methanol and ethanol measured at ground level were characterized by a bimodal
331 pattern with two peaks occurring in the morning (LT 08:00) and evening (LT 20:00),
332 respectively, confirming ~~significant-strong~~ contributions from traffic emissions.
333 However, methanol concentrations measured at 450 m exhibited ~~insignificant-weak~~
334 diurnal variability and lower concentrations on non-working days, indicating that they
335 were less affected by visitor-related emissions. The diurnal profile of ethanol at 450 m
336 displayed two peaks at LT 13:00 and 19:00, respectively, which was in accordance with
337 the two busiest tourist hours of the 450-m platform. In addition, ethanol concentrations
338 at 450 m on non-working days were significantly ($p < 0.01$) higher than those on working
339 days, particularly in the opening hours of the 450-m platform. These results suggest
340 that the ethanol concentrations measured at 450 m were largely contributed by visitor-
341 related emissions.

342 To further explore spatial scales of emission source regions for different VOC
343 species, autocorrelation profiles of their time series were calculated by offsetting time
344 from -120 to 120 min. As indicated in previous studies (Hayes et al., 2013; Hu et al.,
345 2016), ~~concentrations of a species that is~~ more affected by local sources would have a
346 narrower autocorrelation profile. As shown in Figure 4, peak widths of autocorrelation
347 profiles for different ~~chemical-species~~ at 450 m ~~strongly varied-significantly~~.
348 Autocorrelation profiles of monoterpenes, toluene, ethanol, methanol, and isoprene
349 were relatively narrower (even narrower than the autocorrelation profile of NO_x), and
350 thus sources of these species had more local characteristics. Autocorrelation profiles of
351 benzene, C₈ aromatics, acetone, and MVK+MACR were much flatter (but narrower
352 than the autocorrelation profile of ozone and O_x), indicating that concentrations of these
353 species were more contributed by sources at larger spatial scales. By contrast, peak
354 widths of the autocorrelation profiles for different ~~chemical-species~~ (except for ethanol)
355 ~~varied insignificantly at ground level and~~ were ~~similar-comparable~~ to that of NO_x.
356 Therefore, concentrations of the selected VOC species were ~~significantly-notably~~

357 contributed by local traffic emissions at ground level but contributed by more complex
358 sources on larger spatial scales at 450 m.

359 **3.3 Impacts of visitor-related emissions on VOCs measurements**

360 As introduced in section 2.1, the CTT campaign was conducted in August-
361 November of 2020, during which visitors were required to wear masks when visiting
362 the CTT and ethanol-containing products were widely used to prevent the spread of the
363 COVID-19 pandemic. For example, medicinal alcohol (75%) spray was widely used to
364 wipe public utilities and 75%-ethanol bacteriostatic gel was extensively used as
365 sanitizer for hands. The total usage of ethanol-containing products was closely
366 associated with the number of visitors. This can be manifested by the Diurnal profiles
367 of some VOC species (e.g., ethanol and monoterpenes) that exhibited similar diurnal
368 variation patterns to that of the number of visitors at the 450-m platform, as shown in
369 Figure 3. In addition, the restaurants are located ~30 m below the observation site and
370 emission intensities of VOCs (e.g., monoterpenes) from cooking-related sources were
371 also closely associated with the number of visitors. Therefore, the VOCs measurements
372 made at the 450-m platform may be inevitably affected by visitor-related emissions,
373 such as human breath, cooking, and volatilization evaporation of ethanol-containing
374 and personal care products (Veres et al., 2013).

375 As shown in Figure 5(a), the diurnal profile of CO₂ measured at 450 m increased
376 between LT 09:00–20:00, which was different from those measured at ground level.
377 The higher CO₂ mixing ratios at 450 m were predominantly contributed by human
378 breath due to the absence of combustion sources. Measured ethanol mixing ratios were
379 well correlated with those of CO₂ ($r^2=0.6236$, $p<0.01$) during the CTT campaign
380 (Figure 5(b)), indicating that ethanol concentrations, as well as its variations, were
381 predominantly determined by the change in the number of visitors on the tower. In
382 addition, the CO₂ mixing ratios on non-working days, especially during the busiest
383 tourist hours, were markedly significantly ($p<0.01$) higher than those on working days.
384 As illustrated in Figure 5, the The 450-m platform was closed during October 13-15 as

385 the result of the influence of Typhoon Kompas. On these days, mixing ratios of ethanol,
386 CO₂, and monoterpenes exhibited similar variation patterns to benzene (a typical tracer
387 of traffic emissions), as shown in Figure 5(c). However, mixing ratios of ethanol, CO₂,
388 and monoterpenes exhibited quite different variation patterns from benzene when the
389 450-m platform was re-open (October 16–21). For instance, mixing ratios of ethanol,
390 CO₂, and monoterpenes generally decreased from LT 12:00 to 18:00 between October
391 13–15, but significantly-markedly increased during the same period between October
392 16–21. Therefore, it can be concluded that the VOCs measurements made at ~~the 450-~~
393 ~~m-platform~~ were significantly affected by visitor-related emissions, which will be
394 quantitatively assessed using the PMF analysis in following sections.

395 **3.4 Source analysis of VOCs measurements**

396 In this study, a five-factor solution for the PMF analysis was chosen as the optimal
397 result. Figure 6 displays source profiles ($m/z \leq 150$, the full range of the mass spectra
398 is shown in Figure S5S7) of the five PMF factors along with average diurnal profiles
399 of their contributions. The five factors were assigned to likely sources of daytime-mixed,
400 visitor-related, vehicular+industrial, regional transport, and volatile chemical product
401 (VCP)-dominated according to characteristics of their source profiles and temporal
402 variations, which are detailedly discussed in the *SI*.

403 The visitor-related source predominantly includes contributions from human
404 breath and volatilization of ethanol-containing and personal care products.
405 Contributions of the visitor-related source had the narrowest autocorrelation profile
406 among the five factors (Figure 6(g)), confirming its most local characteristics. As shown
407 in Figure 7, the visitor-related source had the largest contributions (15.9 ± 19.6 ppb),
408 accounting for 30% of the average TVOC mixing ratio. In addition, contributions of the
409 visitor-related source accounted for a larger fraction of TVOC mixing ratios on non-
410 working days (33%) than those on working days (28%), as shown in Figures 7 and S8.
411 The vehicular+industrial source mainly includes contributions from vehicular exhausts
412 and emissions of various industrial processes. Contributions of the vehicular+industrial

413 source (15.1 ± 18.3 ppb) were comparable to those of the visitor-related source,
414 accounting for 28% of the average TVOC mixing ratio. As ~~also~~-anticipated, the
415 vehicular+industrial source contributed to a smaller fraction of TVOC mixing ratios on
416 non-working days (26%) than those on working days (30%). The VCP-dominated
417 source predominantly includes contributions from the volatilization of VCPs in urban
418 environments. The VCP-dominated source had an average contribution of 5.7 ± 5.4 ppb,
419 accounting for 11% of the average TVOC mixing ratio. The average contribution of the
420 VCP-dominated source in this study was comparable to those (~ 6.0 ppb) measured in
421 New York City (Gkatzelis et al., 2021). However, VCPs contributed to over 50% of
422 anthropogenic VOCs emissions in New York City, which is significantly much greater
423 than the fraction in this study (11%, and it will increase to 16% when contributions of
424 the visitor-related source were removed). In comparison to large cities in U.S., traffic
425 and industrial emissions were still dominant sources of ambient VOCs in Chinese cities.
426 However, VCPs emissions should also be given more attention as the VCP-dominated
427 (22%) and vehicular+industrial (23%) sources had comparable contributions to the total
428 OH reactivities, as shown in Figure 7(f).

429 The daytime-mixed source predominantly includes contributions from biogenic
430 emissions and photooxidation products of various VOCs. ~~As shown in Figure 7, t~~The
431 daytime-mixed source had an average contribution of 11.6 ± 12.6 ppb, accounting for
432 21% of the average TVOC mixing ratio. It exhibited consistent diurnal variation
433 patterns on both working and non-working days but had larger contributions in the
434 daytime on non-working days (Figure 6). This may be attributed to the enhanced
435 formation of secondary OVOC species as manifested by the higher ozone
436 concentrations on non-working days (Figure ~~S6S9~~). The regional transport source
437 mainly includes contributions from advection transport of aged air masses.
438 Contributions of the regional transport source had the flattest autocorrelation profile
439 ~~(Figure 6)~~, implying its most regional characteristics. Only a small fraction (<5%) of
440 reactive chemical species such as aromatics were attributed to this factor, leading to the

441 lowest contribution to the total OH reactivity. Contributions of the regional transport
442 source accounted for 13% of the TVOC mixing ratio when affected by continental
443 airflows, but only accounted for 3% when affected by marine airflows (Figure [S7S10](#)).
444 By contrast, contributions of the other factors displayed insignificant–weak
445 dependences on wind direction.

446 As shown in Figure 8, source apportionment of the selected VOC species (Figure
447 3) discussed in section 3.2 were further investigated. The vehicular+industrial source
448 had the largest contribution (36%) to benzene. The daytime-mixed source also
449 contributed to 18% of measured benzene mixing ratios. In addition, more than 20% of
450 benzene was attributed to the VCP-dominated source. In contrast to benzene, toluene
451 was predominantly attributed to the vehicular+industrial (93%) and visitor-related (7%)
452 sources. The average ratio of toluene to benzene was 5.7 ppb/ppb during the CTT
453 campaign (Figure [S8S11](#)), further confirming primary contributions of toluene from
454 vehicular and industrial emissions (Wu et al., 2016; Zhou et al., 2019; Xia et al., 2021).
455 The vehicular+industrial source also accounted for the largest fractions of C8 and C9
456 aromatics. In addition, 26% of C8 aromatics and 38% of C9 aromatics were attributed
457 to the VCP-dominated source. The other three sources in total contributed to less than
458 10% of concentrations of C8 and C9 aromatics. These results indicate that VCPs are
459 important sources of aromatics in urban environments but they were rarely identified
460 in previous studies.

461 Isoprene and monoterpenes are widely known tracers of biogenic emissions
462 (Millet et al., 2016; Zhao et al., 2021). However, the daytime-mixed source only
463 contributed to 16% of measured isoprene mixing ratios. By contrast, more than 70% of
464 isoprene were attributed to the visitor-related (38%) and VCP-dominated (35%) sources.
465 As for monoterpenes, more than 95% of the measured mixing ratios were attributed to
466 the visitor-related (47%) and VCP-dominated (49%) sources. The average ratio of
467 monoterpene to isoprene mixing ratios at 450 m was 0.84 in the daytime (LT 08:00–
468 18:00), which was significantly ($p < 0.01$) greater than that at the ground level (0.05)

469 (Figure S8S11). It further confirms ~~significant~~ strong contributions of monoterpenes
470 from visitor-related emissions at the 450-m platform. The daytime-mixed source did
471 not exhibit discernible contributions to monoterpenes. This agrees well with the results
472 in New York City where monoterpene mixing ratios were primarily attributed to
473 anthropogenic sources such as VCPs, cooking, and building materials (Coggon et al.,
474 2021; Gkatzelis et al., 2021). These results suggest that emission intensities of isoprene
475 and monoterpenes may be highly underestimated in urban regions if their anthropogenic
476 emissions are overlooked or less considered. This is exceedingly important for air
477 quality models when estimating formation of ozone and secondary organic aerosol
478 driven by the oxidation of isoprene and monoterpene. As the key photooxidation
479 products of isoprene, nearly 60% of MVK+MACR were attributed to the daytime-
480 mixed source. The visitor-related, regional transport, and VCP-dominated sources
481 contributed to comparable fractions (11%–15%) of MVK+MACR. Therefore,
482 anthropogenic emissions are also important sources of MVK+MACR in urban
483 environments.

484 As shown in Figure 8, 39% of acetone was attributed to the daytime-mixed source.
485 The vehicular+industrial (19%) and VCP-dominated (21%) sources accounted for
486 comparable fractions of measured acetone mixing ratios. ~~In addition, t~~The visitor-
487 related source ~~also had the lowest contribution contributed~~ (7%) ~~significantly~~ to acetone.
488 As for methanol, the vehicular+industrial source accounted for the largest fraction
489 (38%), followed by the daytime-mixed (22%), regional transport (17%), VCP-
490 dominated (14%), and visitor-related (9%) sources. These results reveal that VCPs also
491 contributed significantly to ambient concentrations of acetone and methanol and should
492 be carefully considered when estimating their total emission intensities from
493 anthropogenic sources. Ethanol was predominantly attributed to the visitor-related
494 source. Therefore, the enhanced ethanol mixing ratios were not capable of representing
495 its characteristic concentrations in urban environments. Although the absence of
496 synchronous ground-level measurements, we can speculate that ethanol concentrations

497 at ground level were also ~~significantly~~ increased during the outbreak of the COVID-19
498 pandemic due to the extensive usage of ethanol-containing products. The enhancement
499 of ethanol concentrations ~~may~~ can contribute significantly to the increase in
500 atmospheric OH reactivity (Millet et al., 2012; de Gouw et al., 2017; de Gouw et al.,
501 2018) and then regulate the formation of secondary pollutants. Therefore, impacts of
502 the ethanol enhancement on ambient air quality should be explicitly investigated in
503 future studies due to the wide report of ozone enhancement during the outbreak of the
504 COVID-19 pandemic (Huang et al., 2020; Qi et al., 2021).

505 Acetonitrile is widely used as a typical tracer of biomass burning sources in
506 previous studies (de Gouw et al., 2003b; Zhang et al., 2020; Tan et al., 2021). However,
507 biomass burning source was not identified in this study because acetonitrile was not
508 predominantly attributed to a single factor (~~Figure 8~~). In addition to the visitor-related
509 source, the other four sources also had ~~significant~~ large contributions to acetonitrile. As
510 indicated by (Huangfu et al., 2021), it is not always suitable, particularly in urban
511 environments, to use absolute concentrations of acetonitrile as the indication of biomass
512 burning sources. The ratio of acetonitrile to CO is a better indicator to identify whether
513 VOCs measurements are ~~significantly~~ predominantly contributed by biomass burning
514 emissions. The average ratio of acetonitrile to CO was only 0.09 (ppb ppm⁻¹) during the
515 CTT campaign (Figure S8S11), indicating ~~insignificant~~ negligible contributions from
516 biomass burning sources. In addition to the daytime-mixed (22%) and
517 vehicular+industrial (26%) sources, the VCP-dominated source (31%) ~~was also an~~
518 ~~important source of~~ had large contributions to acetonitrile in urban environments.

519 3.5 Vertical distributions of air pollutants concentrations

520 As introduced in section 2.1, hourly concentrations of some air pollutants were
521 routinely measured at four automatic sites on the CTT. Figure 9 shows ~~time~~
522 series contour plots of vertical profiles of NO_x, ozone, O_x (O₃+NO₂), and PM_{2.5}
523 concentrations in September 2020. Concentrations of the four pollutants all exhibited
524 ~~significantly~~ stratified structures between 488 m and the ground level. Higher mixing

525 ratios of ozone and Ox predominantly occurred at higher altitudes, while higher NOx
526 mixing ratios mainly occurred at ground level. By contrast, higher PM_{2.5} concentrations
527 were observed at both middle altitudes and ground level.

528 To further clarify vertical distribution patterns of air pollutants concentrations,
529 their composite profiles for daytime (LT 08:00–18:00), nighttime (LT 19:00–05:00),
530 and the whole day in the campaign were determined, respectively, as shown in Figure
531 10. Vertical profiles of air pollutants concentrations exhibited similar shapes both in
532 daytime and nighttime. NOx mixing ratios decreased from the ground level to 488 m,
533 suggesting intensive surface emissions around the CTT. Ozone mixing ratios rapidly
534 increased from the ground level to 488 m, which was consistent with the results reported
535 in previous studies (Velasco et al., 2008; Li et al., 2018; Zhang et al., 2019; Li et al.,
536 2021b). The positive gradients of ozone profiles are mainly caused by enhanced NO
537 titration ($\text{NO} + \text{O}_3 = \text{O}_2 + \text{NO}_2$) and dry deposition near ground. Ox mixing ratios also
538 increased from the ground level to 488 m but exhibited weaker gradients in comparison
539 to ozone. Vertical profiles of PM_{2.5} concentrations exhibited similar shapes to NOx
540 during the campaign. Daily mean concentrations of PM_{2.5} and Ox were well correlated
541 at the four altitudes with *r* values varying in the range of 0.61–0.82, suggesting
542 prominent contributions of secondary formation to ambient PM concentrations.
543 Moreover, the correlation coefficients between Ox and PM_{2.5} concentrations at 488 m
544 (0.82) were greater than those at ground level (0.78), as they were less affected by
545 nearby vehicular emissions. This is consistent with the work by (Yan et al., 2020), who
546 reported that secondary components contributed to ~80% of PM_{2.5} concentrations in
547 PRD over the 2008–2019 period.

548 As shown in Figures 9 and 10, vertical profiles of air pollutants concentrations
549 exhibited weaker gradients in the daytime than in the nighttime. Therefore, the daytime
550 VOCs chemistry may have minor differences between the ground level and the 450-m
551 site due to strong vertical mixing of chemical species in the planetary boundary layer
552 (PBLH>450 m, as shown in Figure S9S12). In the nighttime, the oxidative products

553 (such as organic nitrates and OVOCs) of unsaturated hydrocarbons, predominantly
554 initiated by nitrate radicals (NO_3) and ozone, are also important precursors of secondary
555 aerosol (Warneke et al., 2004; Brown et al., 2011; Ng et al., 2017; Liebmann et al.,
556 2019). However, it is highly challenging to investigate the nighttime VOC_s chemistry
557 with only ground-level measurements due to the rapid removal of NO_3 radicals and
558 ozone by enhanced NO titration ~~in the near-surface atmosphere~~ (Geyer and Stutz, 2004;
559 Stutz et al., 2004; Brown et al., 2007). In this condition, the nocturnal residual layer,
560 separated from nocturnal boundary layer and remained, to a large extent, the chemical
561 composition of the daytime atmosphere, could provide an ideal place for investigating
562 nighttime VOC_s chemistry. Oxidative products of VOCs in the residual layer could be
563 mixed downward with the expansion of the PBL during the daytime (Geyer and Stutz,
564 2004; Stutz et al., 2004; Li et al., 2021a), contributing to the formation of ozone and
565 secondary aerosol at ground level. Investigation of the nighttime VOC_s chemistry was
566 one of the initial purposes of this study. Unfortunately, the 450-m site was rarely located
567 in the nocturnal residual layer during the CTT campaign due to frequent occurrences of
568 cloudy and rainy weather. The average nighttime PBLH in Guangzhou was
569 approximately stabilized at 500 m during the campaign (Figure S9S12), implying
570 ~~significant-notable~~ impacts from surface emissions on the measurements made at 450
571 m.

572 In addition to the measured PBLH data, formation of the residual layer at 450 m
573 could be also identified by comparing differences of ozone mixing ratios between 488
574 m and the ground level. Without fresh NO emissions, ozone mixing ratios in the
575 nocturnal residual layer were markedly higher than at ground level and exhibited
576 ~~insignificant-weak~~ variability throughout the nighttime (Caputi et al., 2019; Udina et
577 al., 2020). By contrast, surface ozone mixing ratios are generally very low (close to
578 zero) due to enhanced titration by freshly emitted NO and strong inhibition of
579 atmospheric vertical mixing (Ma et al., 2011; Chen et al., 2020). In this study, the data
580 collected between September 27–30 was one of the cases discussed above and was used

581 to briefly describe behaviors of some representative VOC species (~~including namely~~
582 ethanol, monoterpene, styrene, phenol, and toluene) at 450 m.

583 As shown in Figure 11, ozone mixing ratios measured at ground level (10.2 ± 10.4
584 ppb) were significantly ($p < 0.01$) lower than those at 488 m (44.2 ± 19.6 ppb) on the
585 nighttime of September 27–30, indicating formation of the nocturnal residual layer
586 lower than 450 m. On the nighttime of September 27–28, ozone mixing ratios at 488 m
587 slightly fluctuated around 46.8 ppb between LT 19:00–00:00 and suddenly decreased
588 to 28.4 ppb at LT 01:00 on September 28. The sudden decrease in ozone ~~at 488 m at~~
589 LT 01:00 was accompanied by slight increases in both NO_x and VOCs but ~~significant~~
590 ~~notable~~ decreases in NO_x and NO at ground level, indicating a transitory intrusion of
591 surface fresh emissions into the residual layer. On September 28, ozone mixing ratios
592 at 488 m slightly decreased from 33.0 to 31.5 ppb from LT 02:00 to 05:00, during which
593 mixing ratios of NO_x and VOCs all decreased in different degrees. The continuous
594 decreases in both toluene and ethanol between LT 02:00–05:00 confirm that the VOCs
595 measurements at 450 m were free of interferences by fresh emissions due to their
596 ~~significant large~~ contributions from vehicular exhausts (Figure 78). Toluene mixing
597 ratios decreased by 43% from LT 02:00 to 05:00, which was ~~significantly~~ larger than
598 those (12–27%) of the other VOC species shown in Figure 11. However, the NO₃
599 reactivity (characterized by reaction rate constants of VOC species to NO₃ radical, k_{NO_3})
600 of toluene ($k_{NO_3} = 7 \times 10^{-17} \text{ cm}^3 \text{ molecule}^{-1} \text{ s}^{-1}$) is exceedingly lower than those of the
601 other unsaturated VOC species (k_{NO_3} varies in the magnitudes of $10^{-12} \text{ cm}^3 \text{ molecule}^{-1}$
602 s^{-1}) (Atkinson and Arey, 2003; Atkinson et al., 2006). Therefore, the decline of
603 unsaturated VOC species in the nocturnal residual layer may not be all attributed to the
604 degradation chemistry initiated by NO₃ radicals or ozone.

605 On the nighttime of September 28–29, the PBLH was higher than 500 m between
606 LT 19:00–00:00, resulting in ~~significant notable~~ decreases in ozone and increases in
607 NO_x and VOCs. As shown in Figure 11, the 450-m site may locate in the residual layer
608 after LT 01:00. However, the rapid decrease in mixing ratios of NO_x and VOCs

609 between LT 01:00–05:00 were not likely caused by chemical removal due to the rapid
610 increase in ozone. Regional transport of aged air masses (characterized by high ozone
611 and low NO_x mixing ratios) may be responsible for the rapid decline in various VOC
612 species in the early morning of September 29. On the nighttime of September 29–30,
613 the 450-m site may be ~~significantly~~ impacted by surface fresh emissions as mixing
614 ratios of ozone, NO_x, and VOCs all decreased between LT 19:00–01:00 and
615 simultaneously increased between LT 02:00–05:00. NO_x and toluene mixing ratios
616 generally increased between LT 12:00–18:00 during September 27–29, which were
617 quite different from their average diurnal variation patterns during the whole campaign
618 (Figures 3 and 4). As discussed above, the 450-m site was located in the nocturnal
619 residual layer during September 27–29. Therefore, emissions of pollutants from surface
620 sources could be mixed upward to the measurement site only when the PBLH was
621 higher than 450 m. Furthermore, the PBL was relatively lower and rapidly shrank in
622 the afternoon, leading to the accumulation of chemical species at 450 m.

623 In summary, the VOCs measurements made by PTR-ToF-MS at the 450-m site
624 ~~could~~ can be used to characterize variations in VOC species from their primary
625 emissions during the nighttime. Nevertheless, the oxidative degradation processes of
626 VOCs in the nighttime were not well captured. It is highly difficult to provide more
627 information on the nighttime chemistry of VOC species solely depending on their
628 temporal variations. We believe that the oxidative degradation of reactive VOC species
629 did occur in the nocturnal residual layer due to the coexistence of high concentrations
630 of NO_x and ozone. Measurement techniques that targeting oxidation products (e.g.,
631 ToF-CIMS) and numerical models should be jointly used to deeply analyze the
632 nighttime chemistry of VOCs in the nocturnal residual layer and quantitatively evaluate
633 their impacts on ambient air quality during the daytime.

634 4 Conclusions

635 Continuous measurements of VOCs mixing ratios were made by PTR-ToF-MS at

636 450 m on the CTT in PRD, China from August 18–November 5, 2020. In addition to
637 some specific VOC species (such as ethanol and monoterpenes) that were intensively
638 emitted by visitor-related sources, mixing ratios of most VOC species at 450 m were
639 generally lower than those at ground level. Due to intensive emissions from visitor-
640 related sources, mixing ratios of some VOC species were significantly higher on non-
641 working days than those on working days. The VOCs mixing ratios measured at 450 m
642 also exhibited different diurnal variations from those at ground level, indicating that
643 they were contributed by more mixed sources at larger spatial scales. Five sources,
644 namely daytime-mixed, visitor-related, vehicular+industrial, regional transport, and
645 VCP-dominated, were determined by the PMF model, contributing to ~~22~~21%, 30%,
646 28%, 10%, and 11% of the average TVOC mixing ratio, respectively. In addition to the
647 daytime-mixed and visitor-related sources, the other three sources all had relatively
648 lower contributions on non-working days than on working days. The VCP-dominated
649 source contributed an average of 5.7 ppb to TVOC mixing ratios, which was
650 comparable to those reported in American cities (Gkatzelis et al., 2021). However, the
651 VCP-dominated source accounted for a much smaller fraction (11%) of measured
652 TVOC mixing ratios in this study than in U.S. cities (>50%). Therefore, the reduction
653 in anthropogenic VOC emissions from traffic and industrial sources are still priorities
654 of current air pollution control for Chinese cities. ~~However, t~~hough smaller fraction
655 of VOCs contributed by VCPs was observed in this study compared to cities in U.S.
656 (McDonald et al., 2018; Gkatzelis et al., 2021), large fractions of key VOC species
657 (such as monoterpenes and some aromatic species) were attributed to the VCP-
658 dominated source. In addition, the VCP-dominated (22%) and vehicular+industrial
659 sources (23%) had comparable contributions to the total OH reactivity. Therefore,
660 VCPs emissions should be given more attentions when making control strategies for
661 VOCs in urban region.~~This may be important for formulating control strategies for~~
662 ~~specific chemical species or when they are used as key tracers of certain emission~~
663 ~~sources.~~

664 The vertical distribution patterns of NO_x, ozone, O_x, and PM_{2.5} concentrations
665 were investigated using measurements made at four different heights on the CTT.
666 Vertical profiles of NO_x and PM_{2.5} generally exhibited negative gradients, while
667 vertical profiles of ozone ~~generally~~ demonstrated positive gradients. In addition, the
668 vertical gradients of air pollutants concentrations were larger in the nighttime than in
669 the daytime, predominantly owing to stronger stability of the nocturnal boundary layer.
670 The 450-m site was rarely located in the nocturnal residual layer as cloudy and rainy
671 weather dominated during the campaign. The selected case ~~indicated~~revealed that the
672 NO₃- or O₃-initiated degradation chemistry may be not the sole path for the removal of
673 unsaturated VOC species in ~~the nocturnal residual layer~~nighttime. The degradation
674 chemistry of reactive VOC species in the nocturnal residual layer and their impacts on
675 ground-level air quality could be further investigated in combination with model
676 simulations in future studies.

677 **Data availability**

678 The observational data used in this study are available from corresponding authors
679 upon request.

680 **Author contributions**

681 XBL and BY designed the research. XBL, BY, SHW, CLW, JL, ZJL, XJH, YBHF,
682 CLP, CP, JPQ, CHW, YCY, MC, HDZ, WDY, XMW, and MS contributed to the data
683 collection and data analysis. XBL and BY performed the PMF analysis with
684 contributions from YXS, SXY, and SH. XBL and BY wrote the paper. All the coauthors
685 discussed the results and reviewed the paper.

686 **Competing interests**

687 The authors declare that they have no conflict of interest.

688 **Acknowledgments**

689 This work was financially supported by the National Key R&D Plan of China (grant
690 No. 2019YFE0106300), Guangdong Natural Science Funds for Distinguished Young
691 Scholar (grant No. 2018B030306037), the National Natural Science Foundation of
692 China (grant No. 41877302, 42121004), Key-Area Research and Development
693 Program of Guangdong Province (grant No. 2020B1111360003), China Postdoctoral
694 Science Foundation (grant No. 2019M663367), Guangdong Innovative and
695 Entrepreneurial Research Team Program (grant No. 2016ZT06N263), and Special Fund
696 Project for Science and Technology Innovation Strategy of Guangdong Province (grant
697 No. 2019B121205004). [We sincerely appreciate the help and support from the Canton
698 Tower Management Team.](#)

699 **References**

- 700 An, J., Huang, Y., Huang, C., Wang, X., Yan, R., Wang, Q., Wang, H., Jing, S.,
701 Zhang, Y., Liu, Y., Chen, Y., Xu, C., Qiao, L., Zhou, M., Zhu, S., Hu, Q., Lu, J., and
702 Chen, C.: Emission inventory of air pollutants and chemical speciation for specific
703 anthropogenic sources based on local measurements in the Yangtze River Delta region,
704 China, *Atmos. Chem. Phys.*, 21, 2003-2025, <https://doi.org/10.5194/acp-21-2003-2021>,
705 2021.
- 706 Atkinson, R., and Arey, J.: Atmospheric Degradation of Volatile Organic
707 Compounds, *Chem Rev*, 103, 4605-4638, <https://doi.org/10.1021/cr0206420>, 2003.
- 708 Atkinson, R., Baulch, D. L., Cox, R. A., Crowley, J. N., Hampson, R. F., Hynes,
709 R. G., Jenkin, M. E., Rossi, M. J., Troe, J., and Subcommittee, I.: Evaluated kinetic and
710 photochemical data for atmospheric chemistry: Volume II – gas phase reactions
711 of organic species, *Atmos. Chem. Phys.*, 6, 3625-4055, [https://doi.org/10.5194/acp-6-](https://doi.org/10.5194/acp-6-3625-2006)
712 [3625-2006](https://doi.org/10.5194/acp-6-3625-2006), 2006.
- 713 Baudic, A., Gros, V., Sauvage, S., Locoge, N., Sanchez, O., Sarda-Estève, R.,
714 Kalogridis, C., Petit, J. E., Bonnaire, N., Baisnée, D., Favez, O., Albinet, A., Sciare, J.,
715 and Bonsang, B.: Seasonal variability and source apportionment of volatile organic
716 compounds (VOCs) in the Paris megacity (France), *Atmos. Chem. Phys.*, 16, 11961-
717 11989, <https://doi.org/10.5194/acp-16-11961-2016>, 2016.
- 718 Benish, S. E., He, H., Ren, X., Roberts, S. J., Salawitch, R. J., Li, Z., Wang, F.,
719 Wang, Y., Zhang, F., Shao, M., Lu, S., and Dickerson, R. R.: Measurement report:
720 Aircraft observations of ozone, nitrogen oxides, and volatile organic compounds over
721 Hebei Province, China, *Atmos. Chem. Phys.*, 20, 14523-14545,
722 <https://doi.org/10.5194/acp-20-14523-2020>, 2020.
- 723 Brown, S. S., Dubé, W. P., Osthoff, H. D., Stutz, J., Ryerson, T. B., Wollny, A. G.,
724 Brock, C. A., Warneke, C., de Gouw, J. A., Atlas, E., Neuman, J. A., Holloway, J. S.,
725 Lerner, B. M., Williams, E. J., Kuster, W. C., Goldan, P. D., Angevine, W. M., Trainer,
726 M., Fehsenfeld, F. C., and Ravishankara, A. R.: Vertical profiles in NO₃ and N₂O₅
727 measured from an aircraft: Results from the NOAA P-3 and surface platforms during
728 the New England Air Quality Study 2004, *Journal of Geophysical Research:*
729 *Atmospheres*, 112, <https://doi.org/10.1029/2007JD008883>, 2007.
- 730 Brown, S. S., Dubé, W. P., Peischl, J., Ryerson, T. B., Atlas, E., Warneke, C., de
731 Gouw, J. A., te Lintel Hekkert, S., Brock, C. A., Flocke, F., Trainer, M., Parrish, D. D.,
732 Fehsenfeld, F. C., and Ravishankara, A. R.: Budgets for nocturnal VOC oxidation by
733 nitrate radicals aloft during the 2006 Texas Air Quality Study, *Journal of Geophysical*
734 *Research: Atmospheres*, 116, <https://doi.org/10.1029/2011JD016544>, 2011.
- 735 Caputi, D. J., Faloona, I., Trousdell, J., Smoot, J., Falk, N., and Conley, S.:
736 Residual layer ozone, mixing, and the nocturnal jet in California's San Joaquin Valley,
737 *Atmos. Chem. Phys.*, 19, 4721-4740, <https://doi.org/10.5194/acp-19-4721-2019>, 2019.
- 738 Chen, Q., Li, X.-B., Song, R., Wang, H.-W., Li, B., He, H.-D., and Peng, Z.-R.:

739 Development and utilization of hexacopter unmanned aerial vehicle platform to
740 characterize vertical distribution of boundary layer ozone in wintertime, *Atmospheric*
741 *Pollution Research*, 11, 1073-1083, <https://doi.org/10.1016/j.apr.2020.04.002>, 2020.

742 Chen, X., Millet, D. B., Singh, H. B., Wisthaler, A., Apel, E. C., Atlas, E. L., Blake,
743 D. R., Bourgeois, I., Brown, S. S., Crounse, J. D., de Gouw, J. A., Flocke, F. M., Fried,
744 A., Heikes, B. G., Hornbrook, R. S., Mikoviny, T., Min, K. E., Müller, M., Neuman, J.
745 A., O'Sullivan, D. W., Peischl, J., Pfister, G. G., Richter, D., Roberts, J. M., Ryerson, T.
746 B., Shertz, S. R., Thompson, C. R., Treadaway, V., Veres, P. R., Walega, J., Warneke,
747 C., Washenfelder, R. A., Weibring, P., and Yuan, B.: On the sources and sinks of
748 atmospheric VOCs: an integrated analysis of recent aircraft campaigns over North
749 America, *Atmos. Chem. Phys.*, 19, 9097-9123, [https://doi.org/10.5194/acp-19-9097-](https://doi.org/10.5194/acp-19-9097-2019)
750 [2019](https://doi.org/10.5194/acp-19-9097-2019), 2019.

751 Coggon, M. M., Gkatzelis, G. I., McDonald, B. C., Gilman, J. B., Schwantes, R.
752 H., Abuhassan, N., Aikin, K. C., Arend, M. F., Berkoff, T. A., Brown, S. S., Campos, T.
753 L., Dickerson, R. R., Gronoff, G., Hurley, J. F., Isaacman-VanWertz, G., Koss, A. R.,
754 Li, M., McKeen, S. A., Moshary, F., Peischl, J., Pospisilova, V., Ren, X., Wilson, A.,
755 Wu, Y., Trainer, M., and Warneke, C.: Volatile chemical product emissions enhance
756 ozone and modulate urban chemistry, *Proceedings of the National Academy of Sciences*,
757 118, e2026653118, <https://doi.org/10.1073/pnas.2026653118>, 2021.

758 de Gouw, J., and Warneke, C.: Measurements of volatile organic compounds in the
759 earth's atmosphere using proton-transfer-reaction mass spectrometry, *Mass Spectrom*
760 *Rev*, 26, 223-257, <https://doi.org/10.1002/mas.20119>, 2007.

761 de Gouw, J. A., Goldan, P. D., Warneke, C., Kuster, W. C., Roberts, J. M.,
762 Marchewka, M., Bertman, S. B., Pszenny, A. A. P., and Keene, W. C.: Validation of
763 proton transfer reaction-mass spectrometry (PTR-MS) measurements of gas-phase
764 organic compounds in the atmosphere during the New England Air Quality Study
765 (NEAQS) in 2002, *Journal of Geophysical Research: Atmospheres*, 108,
766 <https://doi.org/10.1029/2003jd003863>, 2003a.

767 de Gouw, J. A., Warneke, C., Parrish, D. D., Holloway, J. S., Trainer, M., and
768 Fehsenfeld, F. C.: Emission sources and ocean uptake of acetonitrile (CH₃CN) in the
769 atmosphere, *Journal of Geophysical Research: Atmospheres*, 108,
770 <https://doi.org/10.1029/2002JD002897>, 2003b.

771 de Gouw, J. A., Gilman, J. B., Kim, S.-W., Lerner, B. M., Isaacman-VanWertz, G.,
772 McDonald, B. C., Warneke, C., Kuster, W. C., Lefer, B. L., Griffith, S. M., Dusanter,
773 S., Stevens, P. S., and Stutz, J.: Chemistry of Volatile Organic Compounds in the Los
774 Angeles basin: Nighttime Removal of Alkenes and Determination of Emission Ratios,
775 *Journal of Geophysical Research: Atmospheres*, 122, 11,843-811,861,
776 <https://doi.org/10.1002/2017JD027459>, 2017.

777 de Gouw, J. A., Gilman, J. B., Kim, S.-W., Alvarez, S. L., Dusanter, S., Graus, M.,
778 Griffith, S. M., Isaacman-VanWertz, G., Kuster, W. C., Lefer, B. L., Lerner, B. M.,
779 McDonald, B. C., Rappenglück, B., Roberts, J. M., Stevens, P. S., Stutz, J., Thalman,
780 R., Veres, P. R., Volkamer, R., Warneke, C., Washenfelder, R. A., and Young, C. J.:

781 Chemistry of Volatile Organic Compounds in the Los Angeles Basin: Formation of
782 Oxygenated Compounds and Determination of Emission Ratios, *Journal of*
783 *Geophysical Research: Atmospheres*, 123, 2298-2319,
784 <https://doi.org/10.1002/2017JD027976>, 2018.

785 Deming, B. L., Pagonis, D., Liu, X., Day, D. A., Talukdar, R., Krechmer, J. E., de
786 Gouw, J. A., Jimenez, J. L., and Ziemann, P. J.: Measurements of delays of gas-phase
787 compounds in a wide variety of tubing materials due to gas-wall interactions, *Atmos.*
788 *Meas. Tech.*, 12, 3453-3461, 10.5194/amt-12-3453-2019, 2019.

789 Dieu Hien, V. T., Lin, C., Thanh, V. C., Kim Oanh, N. T., Thanh, B. X., Weng, C.-
790 E., Yuan, C.-S., and Rene, E. R.: An overview of the development of vertical sampling
791 technologies for ambient volatile organic compounds (VOCs), *J Environ Manage*, 247,
792 401-412, <https://doi.org/10.1016/j.jenvman.2019.06.090>, 2019.

793 Fan, M.-Y., Zhang, Y.-L., Lin, Y.-C., Li, L., Xie, F., Hu, J., Mozaffar, A., and Cao,
794 F.: Source apportionments of atmospheric volatile organic compounds in Nanjing,
795 China during high ozone pollution season, *Chemosphere*, 263, 128025,
796 <https://doi.org/10.1016/j.chemosphere.2020.128025>, 2021.

797 Fry, J. L., Brown, S. S., Middlebrook, A. M., Edwards, P. M., Campuzano-Jost, P.,
798 Day, D. A., Jimenez, J. L., Allen, H. M., Ryerson, T. B., Pollack, I., Graus, M., Warneke,
799 C., de Gouw, J. A., Brock, C. A., Gilman, J., Lerner, B. M., Dubé, W. P., Liao, J., and
800 Welti, A.: Secondary organic aerosol (SOA) yields from NO₃ radical + isoprene based
801 on nighttime aircraft power plant plume transects, *Atmos. Chem. Phys.*, 18, 11663-
802 11682, <https://doi.org/10.5194/acp-18-11663-2018>, 2018.

803 Geng, F., Zhang, Q., Tie, X., Huang, M., Ma, X., Deng, Z., Yu, Q., Quan, J., and
804 Zhao, C.: Aircraft measurements of O₃, NO_x, CO, VOCs, and SO₂ in the Yangtze River
805 Delta region, *Atmos Environ*, 43, 584-593,
806 <https://doi.org/10.1016/j.atmosenv.2008.10.021>, 2009.

807 Geyer, A., and Stutz, J.: Vertical profiles of NO₃, N₂O₅, O₃, and NO_x in the
808 nocturnal boundary layer: 2. Model studies on the altitude dependence of composition
809 and chemistry, *Journal of Geophysical Research: Atmospheres*, 109,
810 <https://doi.org/10.1029/2003jd004211>, 2004.

811 Gkatzelis, G. I., Coggon, M. M., McDonald, B. C., Peischl, J., Gilman, J. B., Aikin,
812 K. C., Robinson, M. A., Canonaco, F., Prevot, A. S. H., Trainer, M., and Warneke, C.:
813 Observations Confirm that Volatile Chemical Products Are a Major Source of
814 Petrochemical Emissions in U.S. Cities, *Environ Sci Technol*,
815 <https://doi.org/10.1021/acs.est.0c05471>, 2021.

816 Gómez, M. C., Durana, N., García, J. A., de Blas, M., Sáez de Cámara, E., García-
817 Ruiz, E., Gangoiti, G., Torre-Pascual, E., and Iza, J.: Long-term measurement of
818 biogenic volatile organic compounds in a rural background area: Contribution to ozone
819 formation, *Atmos Environ*, 224, 117315,
820 <https://doi.org/10.1016/j.atmosenv.2020.117315>, 2020.

821 Greenberg, J. P., Guenther, A., Zimmerman, P., Baugh, W., Geron, C., Davis, K.,
822 Helmig, D., and Klingler, L. F.: Tethered balloon measurements of biogenic VOCs in

823 the atmospheric boundary layer, *Atmos Environ*, 33, 855-867,
824 [https://doi.org/10.1016/S1352-2310\(98\)00302-1](https://doi.org/10.1016/S1352-2310(98)00302-1), 1999.

825 Guo, H., Cheng, H. R., Ling, Z. H., Louie, P. K. K., and Ayoko, G. A.: Which
826 emission sources are responsible for the volatile organic compounds in the atmosphere
827 of Pearl River Delta?, *J Hazard Mater*, 188, 116-124,
828 <https://doi.org/10.1016/j.jhazmat.2011.01.081>, 2011.

829 Hayes, P. L., Ortega, A. M., Cubison, M. J., Froyd, K. D., Zhao, Y., Cliff, S. S.,
830 Hu, W. W., Toohey, D. W., Flynn, J. H., Lefer, B. L., Grossberg, N., Alvarez, S.,
831 Rappenglück, B., Taylor, J. W., Allan, J. D., Holloway, J. S., Gilman, J. B., Kuster, W.
832 C., de Gouw, J. A., Massoli, P., Zhang, X., Liu, J., Weber, R. J., Corrigan, A. L., Russell,
833 L. M., Isaacman, G., Worton, D. R., Kreisberg, N. M., Goldstein, A. H., Thalman, R.,
834 Waxman, E. M., Volkamer, R., Lin, Y. H., Surratt, J. D., Kleindienst, T. E., Offenberg,
835 J. H., Dusanter, S., Griffith, S., Stevens, P. S., Brioude, J., Angevine, W. M., and
836 Jimenez, J. L.: Organic aerosol composition and sources in Pasadena, California, during
837 the 2010 CalNex campaign, *Journal of Geophysical Research: Atmospheres*, 118, 9233-
838 9257, <https://doi.org/10.1002/jgrd.50530>, 2013.

839 He, X., Yuan, B., Wu, C., Wang, S., Wang, C., Huangfu, Y., Qi, J., Ma, N., Xu, W.,
840 Wang, M., Chen, W., Su, H., Cheng, Y., and Shao, M.: Volatile organic compounds in
841 wintertime North China Plain: Insights from measurements of proton transfer reaction
842 time-of-flight mass spectrometer (PTR-ToF-MS), *Journal of Environmental Sciences*,
843 <https://doi.org/10.1016/j.jes.2021.08.010>, 2022.

844 Hornbrook, R. S., Blake, D. R., Diskin, G. S., Fried, A., Fuelberg, H. E., Meinardi,
845 S., Mikoviny, T., Richter, D., Sachse, G. W., Vay, S. A., Walega, J., Weibring, P.,
846 Weinheimer, A. J., Wiedinmyer, C., Wisthaler, A., Hills, A., Riemer, D. D., and Apel, E.
847 C.: Observations of nonmethane organic compounds during ARCTAS − Part 1:
848 Biomass burning emissions and plume enhancements, *Atmos. Chem. Phys.*, 11, 11103-
849 11130, 10.5194/acp-11-11103-2011, 2011.

850 Hu, L., Millet, D. B., Mohr, M. J., Wells, K. C., Griffis, T. J., and Helmig, D.:
851 Sources and seasonality of atmospheric methanol based on tall tower measurements in
852 the US Upper Midwest, *Atmos. Chem. Phys.*, 11, 11145-11156,
853 <https://doi.org/10.5194/acp-11-11145-2011>, 2011.

854 Hu, L., Millet, D. B., Kim, S. Y., Wells, K. C., Griffis, T. J., Fischer, E. V., Helmig,
855 D., Hueber, J., and Curtis, A. J.: North American acetone sources determined from tall
856 tower measurements and inverse modeling, *Atmos. Chem. Phys.*, 13, 3379-3392,
857 <https://doi.org/10.5194/acp-13-3379-2013>, 2013.

858 Hu, L., Millet, D. B., Baasandorj, M., Griffis, T. J., Travis, K. R., Tessum, C. W.,
859 Marshall, J. D., Reinhart, W. F., Mikoviny, T., Müller, M., Wisthaler, A., Graus, M.,
860 Warneke, C., and de Gouw, J.: Emissions of C6–C8 aromatic compounds in the United
861 States: Constraints from tall tower and aircraft measurements, *Journal of Geophysical
862 Research: Atmospheres*, 120, 826-842, <https://doi.org/10.1002/2014JD022627>, 2015a.

863 Hu, L., Millet, D. B., Baasandorj, M., Griffis, T. J., Turner, P., Helmig, D., Curtis,
864 A. J., and Hueber, J.: Isoprene emissions and impacts over an ecological transition

865 region in the U.S. Upper Midwest inferred from tall tower measurements, *Journal of*
866 *Geophysical Research: Atmospheres*, 120, 3553-3571,
867 <https://doi.org/10.1002/2014jd022732>, 2015b.

868 Hu, W., Hu, M., Hu, W., Jimenez, J. L., Yuan, B., Chen, W., Wang, M., Wu, Y.,
869 Chen, C., Wang, Z., Peng, J., Zeng, L., and Shao, M.: Chemical composition, sources,
870 and aging process of submicron aerosols in Beijing: Contrast between summer and
871 winter, *Journal of Geophysical Research: Atmospheres*, 121, 1955-1977,
872 <https://doi.org/10.1002/2015JD024020>, 2016.

873 Huang, X., Ding, A., Gao, J., Zheng, B., Zhou, D., Qi, X., Tang, R., Wang, J., Ren,
874 C., Nie, W., Chi, X., Xu, Z., Chen, L., Li, Y., Che, F., Pang, N., Wang, H., Tong, D.,
875 Qin, W., Cheng, W., Liu, W., Fu, Q., Liu, B., Chai, F., Davis, S. J., Zhang, Q., and He,
876 K.: Enhanced secondary pollution offset reduction of primary emissions during
877 COVID-19 lockdown in China, *National Science Review*, 8,
878 <https://doi.org/10.1093/nsr/nwaa137>, 2020.

879 Huangfu, Y., Yuan, B., Wang, S., Wu, C., He, X., Qi, J., de Gouw, J., Warneke, C.,
880 Gilman, J. B., Wisthaler, A., Karl, T., Graus, M., Jobson, B. T., and Shao, M.: Revisiting
881 Acetonitrile as Tracer of Biomass Burning in Anthropogenic-Influenced Environments,
882 *Geophys Res Lett*, 48, e2020GL092322, <https://doi.org/10.1029/2020GL092322>, 2021.

883 Jin, X., Li, Z., Wu, T., Wang, Y., Cheng, Y., Su, T., Wei, J., Ren, R., Wu, H., Li, S.,
884 Zhang, D., and Cribb, M.: The different sensitivities of aerosol optical properties to
885 particle concentration, humidity, and hygroscopicity between the surface level and the
886 upper boundary layer in Guangzhou, China, *Sci Total Environ*, 803, 150010,
887 <https://doi.org/10.1016/j.scitotenv.2021.150010>, 2022.

888 Klein, F., Farren, N. J., Bozzetti, C., Daellenbach, K. R., Kilic, D., Kumar, N. K.,
889 Pieber, S. M., Slowik, J. G., Tuthill, R. N., Hamilton, J. F., Baltensperger, U., Prévôt,
890 A. S. H., and El Haddad, I.: Indoor terpene emissions from cooking with herbs and
891 pepper and their secondary organic aerosol production potential, *Scientific Reports*, 6,
892 36623, 10.1038/srep36623, 2016.

893 Koss, A., Yuan, B., Warneke, C., Gilman, J. B., Lerner, B. M., Veres, P. R., Peischl,
894 J., Eilerman, S., Wild, R., Brown, S. S., Thompson, C. R., Ryerson, T., Hanisco, T.,
895 Wolfe, G. M., Clair, J. M. S., Thayer, M., Keutsch, F. N., Murphy, S., and de Gouw, J.:
896 Observations of VOC emissions and photochemical products over US oil- and gas-
897 producing regions using high-resolution H₃O⁺ CIMS (PTR-ToF-MS), *Atmospheric*
898 *Measurement Techniques*, 10, <http://dx.doi.org/10.5194/amt-10-2941-2017>, 2017.

899 Li, X.-B., Wang, D., Lu, Q.-C., Peng, Z.-R., Fu, Q., Hu, X.-M., Huo, J., Xiu, G.,
900 Li, B., Li, C., Wang, D.-S., and Wang, H.: Three-dimensional analysis of ozone and
901 PM_{2.5} distributions obtained by observations of tethered balloon and unmanned aerial
902 vehicle in Shanghai, China, *Stoch Env Res Risk A*, 32, 1189-1203,
903 <https://doi.org/10.1007/s00477-018-1524-2>, 2018.

904 Li, X.-B., Fan, G., Lou, S., Yuan, B., Wang, X., and Shao, M.: Transport and
905 boundary layer interaction contribution to extremely high surface ozone levels in
906 eastern China, *Environ Pollut*, 268, 115804,

907 <https://doi.org/10.1016/j.envpol.2020.115804>, 2021a.

908 Li, X.-B., Peng, Z.-R., Wang, D., Li, B., Huangfu, Y., Fan, G., Wang, H., and Lou,
909 S.: Vertical distributions of boundary-layer ozone and fine aerosol particles during the
910 emission control period of the G20 summit in Shanghai, China, *Atmospheric Pollution*
911 *Research*, 12, 352-364, <https://doi.org/10.1016/j.apr.2020.09.016>, 2021b.

912 Li, X.-B., Yuan, B., Parrish, D. D., Chen, D., Song, Y., Yang, S., Liu, Z., and Shao,
913 M.: Long-term trend of ozone in southern China reveals future mitigation strategy for
914 air pollution, *Atmos Environ*, 269, 118869, [10.1016/j.atmosenv.2021.118869](https://doi.org/10.1016/j.atmosenv.2021.118869), 2022.

915 Liebmann, J., Sobanski, N., Schuladen, J., Karu, E., Hellén, H., Hakola, H., Zha,
916 Q., Ehn, M., Riva, M., Heikkinen, L., Williams, J., Fischer, H., Lelieveld, J., and
917 Crowley, J. N.: Alkyl nitrates in the boreal forest: formation via the NO_3^- , OH^- and O_3 -
918 induced oxidation of biogenic volatile organic compounds and ambient lifetimes,
919 *Atmos. Chem. Phys.*, 19, 10391-10403, <https://doi.org/10.5194/acp-19-10391-2019>,
920 2019.

921 Liu, B., Liang, D., Yang, J., Dai, Q., Bi, X., Feng, Y., Yuan, J., Xiao, Z., Zhang, Y.,
922 and Xu, H.: Characterization and source apportionment of volatile organic compounds
923 based on 1-year of observational data in Tianjin, China, *Environ Pollut*, 218, 757-769,
924 <https://doi.org/10.1016/j.envpol.2016.07.072>, 2016.

925 Liu, X., Deming, B., Pagonis, D., Day, D. A., Palm, B. B., Talukdar, R., Roberts,
926 J. M., Veres, P. R., Krechmer, J. E., Thornton, J. A., de Gouw, J. A., Ziemann, P. J., and
927 Jimenez, J. L.: Effects of gas-wall interactions on measurements of semivolatile
928 compounds and small polar molecules, *Atmos. Meas. Tech.*, 12, 3137-3149,
929 [10.5194/amt-12-3137-2019](https://doi.org/10.5194/amt-12-3137-2019), 2019.

930 Liu, Y., Wang, H., Jing, S., Zhou, M., Lou, S., Qu, K., Qiu, W., Wang, Q., Li, S.,
931 Gao, Y., Liu, Y., Li, X., Peng, Z.-R., Chen, J., and Lu, K.: Vertical Profiles of Volatile
932 Organic Compounds in Suburban Shanghai, *Adv Atmos Sci*, 38, 1177-1187,
933 <https://doi.org/10.1007/s00376-021-0126-y>, 2021.

934 Ma, Z., Zhang, X., Xu, J., Zhao, X., and Meng, W.: Characteristics of ozone
935 vertical profile observed in the boundary layer around Beijing in autumn, *Journal of*
936 *Environmental Sciences*, 23, 1316-1324, [https://doi.org/10.1016/s1001-](https://doi.org/10.1016/s1001-0742(10)60557-8)
937 [0742\(10\)60557-8](https://doi.org/10.1016/s1001-0742(10)60557-8), 2011.

938 McDonald, B. C., de Gouw, J. A., Gilman, J. B., Jathar, S. H., Akherati, A., Cappa,
939 C. D., Jimenez, J. L., Lee-Taylor, J., Hayes, P. L., McKeen, S. A., Cui, Y. Y., Kim, S.-
940 W., Gentner, D. R., Isaacman-VanWertz, G., Goldstein, A. H., Harley, R. A., Frost, G.
941 J., Roberts, J. M., Ryerson, T. B., and Trainer, M.: Volatile chemical products emerging
942 as largest petrochemical source of urban organic emissions, *Science*, 359, 760,
943 <https://doi.org/10.1126/science.aag0524>, 2018.

944 Millet, D. B., Apel, E., Henze, D. K., Hill, J., Marshall, J. D., Singh, H. B., and
945 Tessum, C. W.: Natural and Anthropogenic Ethanol Sources in North America and
946 Potential Atmospheric Impacts of Ethanol Fuel Use, *Environ Sci Technol*, 46, 8484-
947 8492, <https://doi.org/10.1021/es300162u>, 2012.

948 Millet, D. B., Baasandorj, M., Hu, L., Mitroo, D., Turner, J., and Williams, B. J.:

949 Nighttime Chemistry and Morning Isoprene Can Drive Urban Ozone Downwind of a
950 Major Deciduous Forest, *Environ Sci Technol*, 50, 4335-4342,
951 <https://doi.org/10.1021/acs.est.5b06367>, 2016.

952 Mo, Z., Shao, M., and Lu, S.: Compilation of a source profile database for
953 hydrocarbon and OVOC emissions in China, *Atmos Environ*, 143, 209-217,
954 <https://doi.org/10.1016/j.atmosenv.2016.08.025>, 2016.

955 Mo, Z., Huang, S., Yuan, B., Pei, C., Song, Q., Qi, J., Wang, M., Wang, B., Wang,
956 C., Li, M., Zhang, Q., and Shao, M.: Deriving emission fluxes of volatile organic
957 compounds from tower observation in the Pearl River Delta, China, *Sci Total Environ*,
958 741, 139763, <https://doi.org/10.1016/j.scitotenv.2020.139763>, 2020.

959 Müller, M., Anderson, B. E., Beyersdorf, A. J., Crawford, J. H., Diskin, G. S.,
960 Eichler, P., Fried, A., Keutsch, F. N., Mikoviny, T., Thornhill, K. L., Walega, J. G.,
961 Weinheimer, A. J., Yang, M., Yokelson, R. J., and Wisthaler, A.: In situ measurements
962 and modeling of reactive trace gases in a small biomass burning plume, *Atmos. Chem.*
963 *Phys.*, 16, 3813-3824, 10.5194/acp-16-3813-2016, 2016.

964 Ng, N. L., Brown, S. S., Archibald, A. T., Atlas, E., Cohen, R. C., Crowley, J. N.,
965 Day, D. A., Donahue, N. M., Fry, J. L., Fuchs, H., Griffin, R. J., Guzman, M. I.,
966 Herrmann, H., Hodzic, A., Iinuma, Y., Jimenez, J. L., Kiendler-Scharr, A., Lee, B. H.,
967 Luecken, D. J., Mao, J. Q., McLaren, R., Mutzel, A., Osthoff, H. D., Ouyang, B.,
968 Picquet-Varrault, B., Platt, U., Pye, H. O. T., Rudich, Y., Schwantes, R. H., Shiraiwa,
969 M., Stutz, J., Thornton, J. A., Tilgner, A., Williams, B. J., and Zaveri, R. A.: Nitrate
970 radicals and biogenic volatile organic compounds: oxidation, mechanisms, and organic
971 aerosol, *Atmos. Chem. Phys.*, 17, 2103-2162, [https://doi.org/10.5194/acp-17-2103-](https://doi.org/10.5194/acp-17-2103-2017)
972 [2017](https://doi.org/10.5194/acp-17-2103-2017), 2017.

973 Pallavi, Sinha, B., and Sinha, V.: Source apportionment of volatile organic
974 compounds in the northwest Indo-Gangetic Plain using a positive matrix factorization
975 model, *Atmos. Chem. Phys.*, 19, 15467-15482, [https://doi.org/10.5194/acp-19-15467-](https://doi.org/10.5194/acp-19-15467-2019)
976 [2019](https://doi.org/10.5194/acp-19-15467-2019), 2019.

977 Pernov, J. B., Bossi, R., Lebourgeois, T., Nøjgaard, J. K., Holzinger, R., Hjorth, J.
978 L., and Skov, H.: Atmospheric VOC measurements at a High Arctic site: characteristics
979 and source apportionment, *Atmos. Chem. Phys.*, 21, 2895-2916,
980 <https://doi.org/10.5194/acp-21-2895-2021>, 2021.

981 Qi, J., Mo, Z., Yuan, B., Huang, S., Huangfu, Y., Wang, Z., Li, X., Yang, S., Wang,
982 W., Zhao, Y., Wang, X., Wang, W., Liu, K., and Shao, M.: An observation approach in
983 evaluation of ozone production to precursor changes during the COVID-19 lockdown,
984 *Atmos Environ*, 262, 118618, <https://doi.org/10.1016/j.atmosenv.2021.118618>, 2021.

985 Qin, J., Wang, X., Yang, Y., Qin, Y., Shi, S., Xu, P., Chen, R., Zhou, X., Tan, J.,
986 and Wang, X.: Source apportionment of VOCs in a typical medium-sized city in North
987 China Plain and implications on control policy, *Journal of Environmental Sciences*, 107,
988 26-37, <https://doi.org/10.1016/j.jes.2020.10.005>, 2021.

989 Sangiorgi, G., Ferrero, L., Perrone, M. G., Bolzacchini, E., Duane, M., and Larsen,
990 B. R.: Vertical distribution of hydrocarbons in the low troposphere below and above the

991 mixing height: Tethered balloon measurements in Milan, Italy, *Environ Pollut*, 159,
 992 3545-3552, <https://doi.org/10.1016/j.envpol.2011.08.012>, 2011.

993 Squires, F. A., Nemitz, E., Langford, B., Wild, O., Drysdale, W. S., Acton, W. J. F.,
 994 Fu, P., Grimmond, C. S. B., Hamilton, J. F., Hewitt, C. N., Hollaway, M., Kotthaus, S.,
 995 Lee, J., Metzger, S., Pingingtha-Durden, N., Shaw, M., Vaughan, A. R., Wang, X., Wu,
 996 R., Zhang, Q., and Zhang, Y.: Measurements of traffic-dominated pollutant emissions
 997 in a Chinese megacity, *Atmos. Chem. Phys.*, 20, 8737-8761,
 998 <https://doi.org/10.5194/acp-20-8737-2020>, 2020.

999 Stutz, J., Alicke, B., Ackermann, R., Geyer, A., White, A., and Williams, E.:
 1000 Vertical profiles of NO₃, N₂O₅, O₃, and NO_x in the nocturnal boundary layer: 1.
 1001 Observations during the Texas Air Quality Study 2000, *Journal of Geophysical*
 1002 *Research: Atmospheres*, 109, <https://doi.org/10.1029/2003jd004209>, 2004.

1003 Tan, Y., Han, S., Chen, Y., Zhang, Z., Li, H., Li, W., Yuan, Q., Li, X., Wang, T.,
 1004 and Lee, S.-c.: Characteristics and source apportionment of volatile organic compounds
 1005 (VOCs) at a coastal site in Hong Kong, *Sci Total Environ*, 777, 146241,
 1006 <https://doi.org/10.1016/j.scitotenv.2021.146241>, 2021.

1007 Ting, M., Yue-si, W., Jie, J., Fang-kun, W., and Mingxing, W.: The vertical
 1008 distributions of VOCs in the atmosphere of Beijing in autumn, *Sci Total Environ*, 390,
 1009 97-108, <https://doi.org/10.1016/j.scitotenv.2007.08.035>, 2008.

1010 Udina, M., Soler, M. R., Olid, M., Jiménez-Esteve, B., and Bech, J.: Pollutant
 1011 vertical mixing in the nocturnal boundary layer enhanced by density currents and low-
 1012 level jets: two representative case studies, *Bound-lay Meteorol*, 174, 203-230,
 1013 <https://doi.org/10.1007/s10546-019-00483-y>, 2020.

1014 Ulbrich, I. M., Canagaratna, M. R., Zhang, Q., Worsnop, D. R., and Jimenez, J. L.:
 1015 Interpretation of organic components from Positive Matrix Factorization of aerosol
 1016 mass spectrometric data, *Atmos. Chem. Phys.*, 9, 2891-2918,
 1017 <https://doi.org/10.5194/acp-9-2891-2009>, 2009.

1018 Velasco, E., Marquez, C., Bueno, E., Bernabe, R. M., Sanchez, A., Fentanes, O.,
 1019 Wohrnschimmel, H., Cardenas, B., Kamilla, A., Wakamatsu, S., and Molina, L. T.:
 1020 Vertical distribution of ozone and VOCs in the low boundary layer of Mexico City,
 1021 *Atmos. Chem. Phys.*, 8, 3061-3079, <https://doi.org/10.5194/acp-8-3061-2008>, 2008.

1022 Veres, P. R., Faber, P., Drewnick, F., Lelieveld, J., and Williams, J.: Anthropogenic
 1023 sources of VOC in a football stadium: Assessing human emissions in the atmosphere,
 1024 *Atmos Environ*, 77, 1052-1059, <https://doi.org/10.1016/j.atmosenv.2013.05.076>, 2013.

1025 Vo, T.-D.-H., Lin, C., Weng, C.-E., Yuan, C.-S., Lee, C.-W., Hung, C.-H., Bui, X.-
 1026 T., Lo, K.-C., and Lin, J.-X.: Vertical stratification of volatile organic compounds and
 1027 their photochemical product formation potential in an industrial urban area, *J Environ*
 1028 *Manage*, 217, 327-336, <https://doi.org/10.1016/j.jenvman.2018.03.101>, 2018.

1029 Wang, C., Yuan, B., Wu, C., Wang, S., Qi, J., Wang, B., Wang, Z., Hu, W., Chen,
 1030 W., Ye, C., Wang, W., Sun, Y., Wang, C., Huang, S., Song, W., Wang, X., Yang, S.,
 1031 Zhang, S., Xu, W., Ma, N., Zhang, Z., Jiang, B., Su, H., Cheng, Y., Wang, X., and Shao,
 1032 M.: Measurements of higher alkanes using NO⁺ chemical ionization in PTR-ToF-MS:

1033 important contributions of higher alkanes to secondary organic aerosols in China,
1034 Atmos. Chem. Phys., 20, 14123-14138, <https://doi.org/10.5194/acp-20-14123-2020>,
1035 2020a.

1036 Wang, T., Xue, L., Brimblecombe, P., Lam, Y. F., Li, L., and Zhang, L.: Ozone
1037 pollution in China: A review of concentrations, meteorological influences, chemical
1038 precursors, and effects, Sci Total Environ, 575, 1582-1596,
1039 <https://doi.org/10.1016/j.scitotenv.2016.10.081>, 2017.

1040 Wang, Y., Wang, Y., Tang, G., Yang, Y., Li, X., Yao, D., Wu, S., Kang, Y., Wang,
1041 M., and Wang, Y.: High gaseous carbonyl concentrations in the upper boundary layer
1042 in Shijiazhuang, China, Sci Total Environ, 799, 149438,
1043 <https://doi.org/10.1016/j.scitotenv.2021.149438>, 2021.

1044 Wang, Y. H., Gao, W. K., Wang, S., Song, T., Gong, Z. Y., Ji, D. S., Wang, L. L.,
1045 Liu, Z. R., Tang, G. Q., Huo, Y. F., Tian, S. L., Li, J. Y., Li, M. G., Yang, Y., Chu, B. W.,
1046 Petaja, T., Kerminen, V. M., He, H., Hao, J. M., Kulmala, M., Wang, Y. S., and Zhang,
1047 Y. H.: Contrasting trends of PM_{2.5} and surface-ozone concentrations in China from 2013
1048 to 2017, National Science Review, 7, 1331-1339, <https://doi.org/10.1093/nsr/nwaa032>,
1049 2020b.

1050 Wang, Z., Yuan, B., Ye, C., Roberts, J., Wisthaler, A., Lin, Y., Li, T., Wu, C., Peng,
1051 Y., Wang, C., Wang, S., Yang, S., Wang, B., Qi, J., Wang, C., Song, W., Hu, W., Wang,
1052 X., Xu, W., Ma, N., Kuang, Y., Tao, J., Zhang, Z., Su, H., Cheng, Y., Wang, X., and
1053 Shao, M.: High Concentrations of Atmospheric Isocyanic Acid (HNCO) Produced from
1054 Secondary Sources in China, Environ Sci Technol, 54, 11818-11826,
1055 <https://doi.org/10.1021/acs.est.0c02843>, 2020c.

1056 Warneke, C., de Gouw, J. A., Goldan, P. D., Kuster, W. C., Williams, E. J., Lerner,
1057 B. M., Jakoubek, R., Brown, S. S., Stark, H., Aldener, M., Ravishankara, A. R., Roberts,
1058 J. M., Marchewka, M., Bertman, S., Sueper, D. T., McKeen, S. A., Meagher, J. F., and
1059 Fehsenfeld, F. C.: Comparison of daytime and nighttime oxidation of biogenic and
1060 anthropogenic VOCs along the New England coast in summer during New England Air
1061 Quality Study 2002, Journal of Geophysical Research: Atmospheres, 109,
1062 <https://doi.org/10.1029/2003jd004424>, 2004.

1063 Wu, C., Wang, C., Wang, S., Wang, W., Yuan, B., Qi, J., Wang, B., Wang, H., Wang,
1064 C., Song, W., Wang, X., Hu, W., Lou, S., Ye, C., Peng, Y., Wang, Z., Huangfu, Y., Xie,
1065 Y., Zhu, M., Zheng, J., Wang, X., Jiang, B., Zhang, Z., and Shao, M.: Measurement
1066 report: Important contributions of oxygenated compounds to emissions and chemistry
1067 of volatile organic compounds in urban air, Atmos. Chem. Phys., 20, 14769-14785,
1068 <https://doi.org/10.5194/acp-20-14769-2020>, 2020a.

1069 Wu, F., Yu, Y., Sun, J., Zhang, J., Wang, J., Tang, G., and Wang, Y.: Characteristics,
1070 source apportionment and reactivity of ambient volatile organic compounds at Dinghu
1071 Mountain in Guangdong Province, China, Sci Total Environ, 548-549, 347-359,
1072 <https://doi.org/10.1016/j.scitotenv.2015.11.069>, 2016.

1073 Wu, S., Tang, G., Wang, Y., Yang, Y., Yao, D., Zhao, W., Gao, W., Sun, J., and
1074 Wang, Y.: Vertically decreased VOC concentration and reactivity in the planetary

1075 boundary layer in winter over the North China Plain, *Atmos Res*, 240, 104930,
1076 <https://doi.org/10.1016/j.atmosres.2020.104930>, 2020b.

1077 Wu, S., Tang, G. Q., Wang, Y. H., Mai, R., Yao, D., Kang, Y. Y., Wang, Q. L., and
1078 Wang, Y. S.: Vertical Evolution of Boundary Layer Volatile Organic Compounds in
1079 Summer over the North China Plain and the Differences with Winter, *Adv Atmos Sci*,
1080 38, 1165-1176, <https://doi.org/10.1007/s00376-020-0254-9>, 2021.

1081 Xia, S.-Y., Wang, C., Zhu, B., Chen, X., Feng, N., Yu, G.-H., and Huang, X.-F.:
1082 Long-term observations of oxygenated volatile organic compounds (OVOCs) in an
1083 urban atmosphere in southern China, 2014–2019, *Environ Pollut*, 270, 116301,
1084 <https://doi.org/10.1016/j.envpol.2020.116301>, 2021.

1085 Xue, L., Wang, T., Simpson, I. J., Ding, A., Gao, J., Blake, D. R., Wang, X., Wang,
1086 W., Lei, H., and Jin, D.: Vertical distributions of non-methane hydrocarbons and
1087 halocarbons in the lower troposphere over northeast China, *Atmos Environ*, 45, 6501-
1088 6509, <https://doi.org/10.1016/j.atmosenv.2011.08.072>, 2011.

1089 Yan, F., Chen, W., Jia, S., Zhong, B., Yang, L., Mao, J., Chang, M., Shao, M., Yuan,
1090 B., Situ, S., Wang, X., Chen, D., and Wang, X.: Stabilization for the secondary species
1091 contribution to PM_{2.5} in the Pearl River Delta (PRD) over the past decade, China: A
1092 meta-analysis, *Atmos Environ*, 242, 117817,
1093 <https://doi.org/10.1016/j.atmosenv.2020.117817>, 2020.

1094 Ye, C., Yuan, B., Lin, Y., Wang, Z., Hu, W., Li, T., Chen, W., Wu, C., Wang, C.,
1095 Huang, S., Qi, J., Wang, B., Wang, C., Song, W., Wang, X., Zheng, E., Krechmer, J. E.,
1096 Ye, P., Zhang, Z., Wang, X., Worsnop, D. R., and Shao, M.: Chemical characterization
1097 of oxygenated organic compounds in the gas phase and particle phase using iodide
1098 CIMS with FIGAERO in urban air, *Atmos. Chem. Phys.*, 21, 8455-8478,
1099 <https://doi.org/10.5194/acp-21-8455-2021>, 2021.

1100 Yuan, B., Shao, M., de Gouw, J., Parrish, D. D., Lu, S., Wang, M., Zeng, L., Zhang,
1101 Q., Song, Y., Zhang, J., and Hu, M.: Volatile organic compounds (VOCs) in urban air:
1102 How chemistry affects the interpretation of positive matrix factorization (PMF) analysis,
1103 *Journal of Geophysical Research: Atmospheres*, 117,
1104 <https://doi.org/10.1029/2012jd018236>, 2012.

1105 Yuan, B., Koss, A., Warneke, C., Gilman, J. B., Lerner, B. M., Stark, H., and de
1106 Gouw, J. A.: A high-resolution time-of-flight chemical ionization mass spectrometer
1107 utilizing hydronium ions (H₃O⁺ ToF-CIMS) for measurements of volatile organic
1108 compounds in the atmosphere, *Atmospheric Measurement Techniques*, 9, 2735-2752,
1109 <https://doi.org/10.5194/amt-9-2735-2016>, 2016.

1110 Yuan, B., Koss, A. R., Warneke, C., Coggon, M., Sekimoto, K., and de Gouw, J.
1111 A.: Proton-Transfer-Reaction Mass Spectrometry: Applications in Atmospheric
1112 Sciences, *Chem Rev*, 117, 13187-13229, <https://doi.org/10.1021/acs.chemrev.7b00325>,
1113 2017.

1114 Yuan, Z., Zhong, L., Lau, A. K. H., Yu, J. Z., and Louie, P. K. K.: Volatile organic
1115 compounds in the Pearl River Delta: Identification of source regions and
1116 recommendations for emission-oriented monitoring strategies, *Atmos Environ*, 76, 162-

1117 172, <https://doi.org/10.1016/j.atmosenv.2012.11.034>, 2013.

1118 Zhang, H., Zhang, Y., Huang, Z., Acton, W. J. F., Wang, Z., Nemitz, E., Langford,
1119 B., Mullinger, N., Davison, B., Shi, Z., Liu, D., Song, W., Yang, W., Zeng, J., Wu, Z.,
1120 Fu, P., Zhang, Q., and Wang, X.: Vertical profiles of biogenic volatile organic
1121 compounds as observed online at a tower in Beijing, *J Environ Sci (China)*, 95, 33-42,
1122 <https://doi.org/10.1016/j.jes.2020.03.032>, 2020.

1123 Zhang, K., Xiu, G., Zhou, L., Bian, Q., Duan, Y., Fei, D., Wang, D., and Fu, Q.:
1124 Vertical distribution of volatile organic compounds within the lower troposphere in late
1125 spring of Shanghai, *Atmos Environ*, 186, 150-157,
1126 <https://doi.org/10.1016/j.atmosenv.2018.03.044>, 2018.

1127 Zhang, K., Zhou, L., Fu, Q., Yan, L., Bian, Q., Wang, D., and Xiu, G.: Vertical
1128 distribution of ozone over Shanghai during late spring: A balloon-borne observation,
1129 *Atmos Environ*, 208, 48-60, <https://doi.org/10.1016/j.atmosenv.2019.03.011>, 2019.

1130 Zhang, Y., Wang, X., Barletta, B., Simpson, I. J., Blake, D. R., Fu, X., Zhang, Z.,
1131 He, Q., Liu, T., Zhao, X., and Ding, X.: Source attributions of hazardous aromatic
1132 hydrocarbons in urban, suburban and rural areas in the Pearl River Delta (PRD) region,
1133 *J Hazard Mater*, 250-251, 403-411, <https://doi.org/10.1016/j.jhazmat.2013.02.023>,
1134 2013.

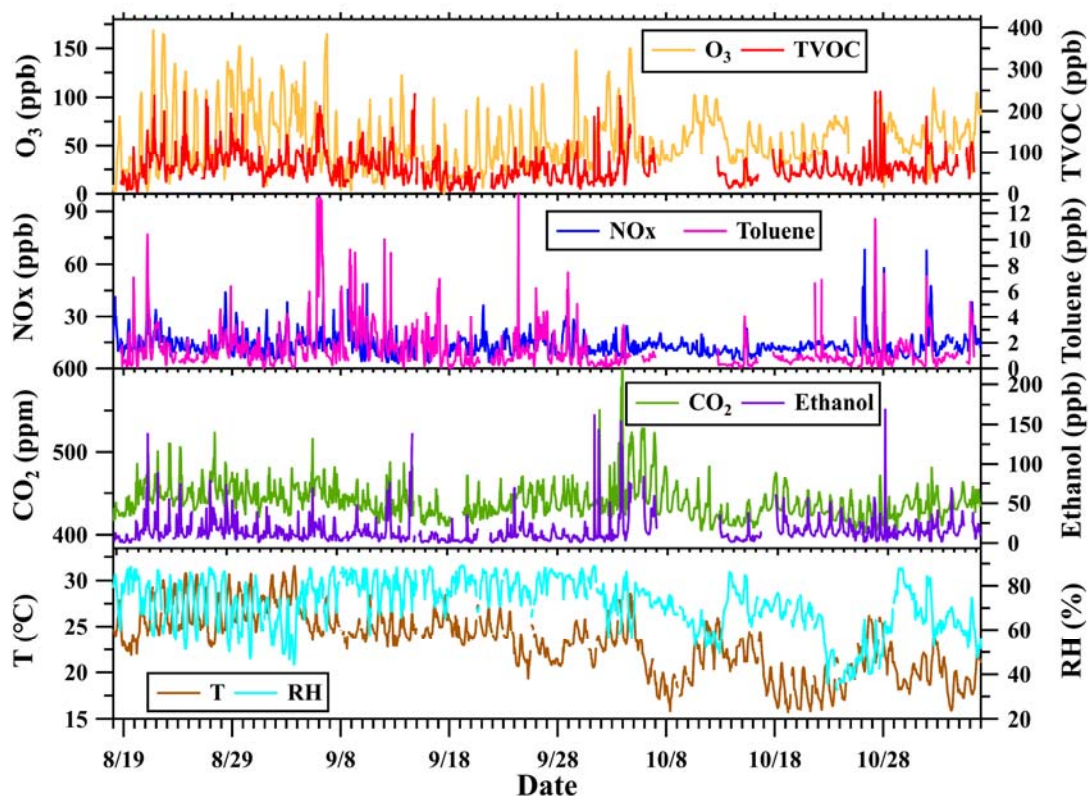
1135 Zhao, D., Pullinen, I., Fuchs, H., Schrade, S., Wu, R., Acir, I. H., Tillmann, R.,
1136 Rohrer, F., Wildt, J., Guo, Y., Kiendler-Scharr, A., Wahner, A., Kang, S., Vereecken, L.,
1137 and Mentel, T. F.: Highly oxygenated organic molecule (HOM) formation in the
1138 isoprene oxidation by NO₃ radical, *Atmos. Chem. Phys.*, 21, 9681-9704,
1139 <https://doi.org/10.5194/acp-21-9681-2021>, 2021.

1140 Zheng, J., Yu, Y., Mo, Z., Zhang, Z., Wang, X., Yin, S., Peng, K., Yang, Y., Feng,
1141 X., and Cai, H.: Industrial sector-based volatile organic compound (VOC) source
1142 profiles measured in manufacturing facilities in the Pearl River Delta, China, *Sci Total*
1143 *Environ*, 456-457, 127-136, <https://doi.org/10.1016/j.scitotenv.2013.03.055>, 2013.

1144 Zhou, X., Li, Z., Zhang, T., Wang, F., Wang, F., Tao, Y., Zhang, X., Wang, F., and
1145 Huang, J.: Volatile organic compounds in a typical petrochemical industrialized valley
1146 city of northwest China based on high-resolution PTR-MS measurements:
1147 Characterization, sources and chemical effects, *Sci Total Environ*, 671, 883-896,
1148 <https://doi.org/10.1016/j.scitotenv.2019.03.283>, 2019.

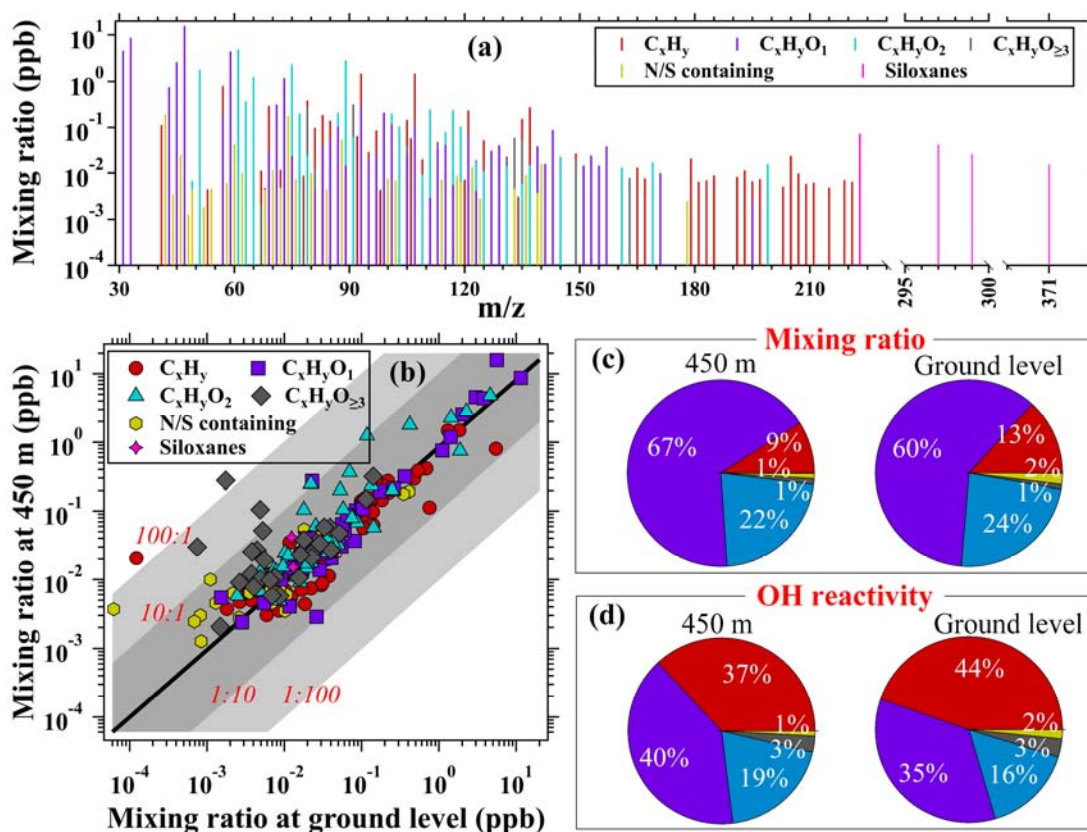
1149 Zhu, B., Han, Y., Wang, C., Huang, X., Xia, S., Niu, Y., Yin, Z., and He, L.:
1150 Understanding primary and secondary sources of ambient oxygenated volatile organic
1151 compounds in Shenzhen utilizing photochemical age-based parameterization method,
1152 *Journal of Environmental Sciences*, 75, 105-114,
1153 <https://doi.org/10.1016/j.jes.2018.03.008>, 2019.

1154



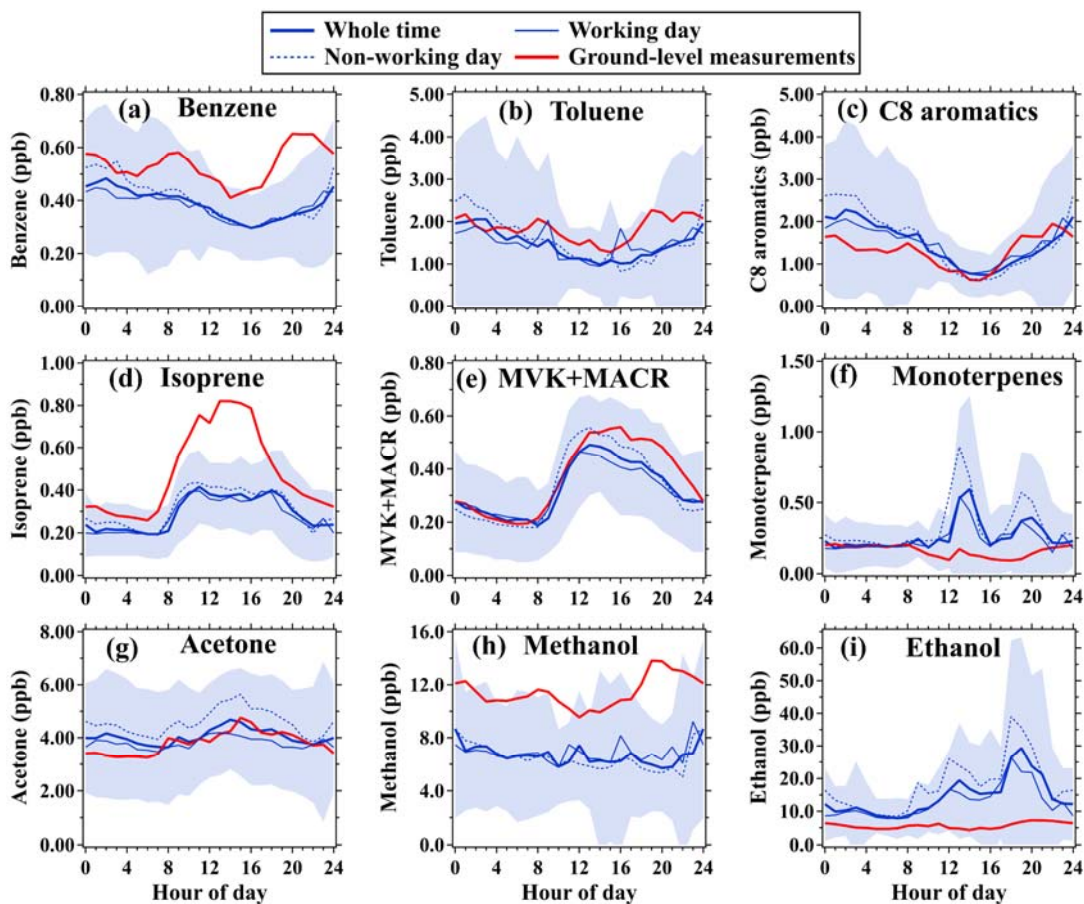
1155

1156 **Figure 1.** Time series of concentrations of some typical chemical species along with
 1157 meteorological parameters (hourly averages) during the CTT campaign. Temperature
 1158 (T), relative humidity (RH), concentrations of ozone and NOx were measured at 488
 1159 m. Concentrations of VOCs, ethanol, and CO₂ were measured at 450 m.



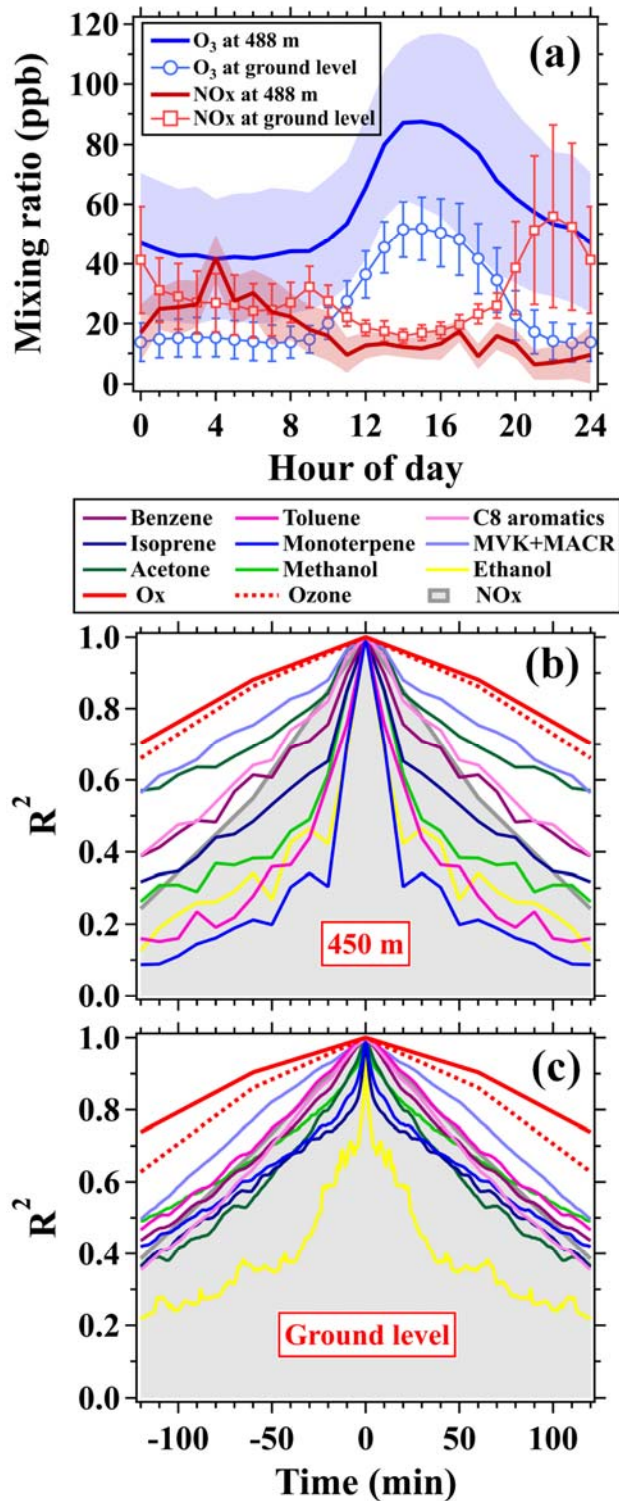
1160

1161 **Figure 2.** (a) Average mass spectra of VOCs (including 225 species) obtained by PTR-
 1162 ToF-MS measured at 450 m during the CTT campaign. (b) Scatter plots of the average
 1163 VOC mixing ratios measured at 450 m during the CTT campaign versus those measured
 1164 at ~~the~~ ground level during the GIG campaign; The black solid line indicates the ratio of
 1165 1:1; The dark grey shaded areas indicate the ratios of 10:1 and 1:10; The light grey
 1166 shaded areas indicate the ratios of 100:1 and 1:100. ~~C_xH_y refers to hydrocarbons.~~
 1167 ~~$C_xH_yO_1$ refers to VOC species containing one oxygen atom. $C_xH_yO_2$ refers to VOC~~
 1168 ~~species containing two oxygen atoms. $C_xH_yO_{\geq 3}$ refers to VOC species containing more~~
 1169 ~~than three oxygen atoms. N/S-containing refers to VOC species containing nitrogen or~~
 1170 ~~sulfur atoms.~~ (c-d) Average contribution percentages of the six VOCs categories to their
 1171 total concentrations and OH reactivities at 450 m and the ground level, respectively;
 1172 Only the VOCs species that have known reaction rate constants with OH radical (Table
 1173 S1) were used for calculation.



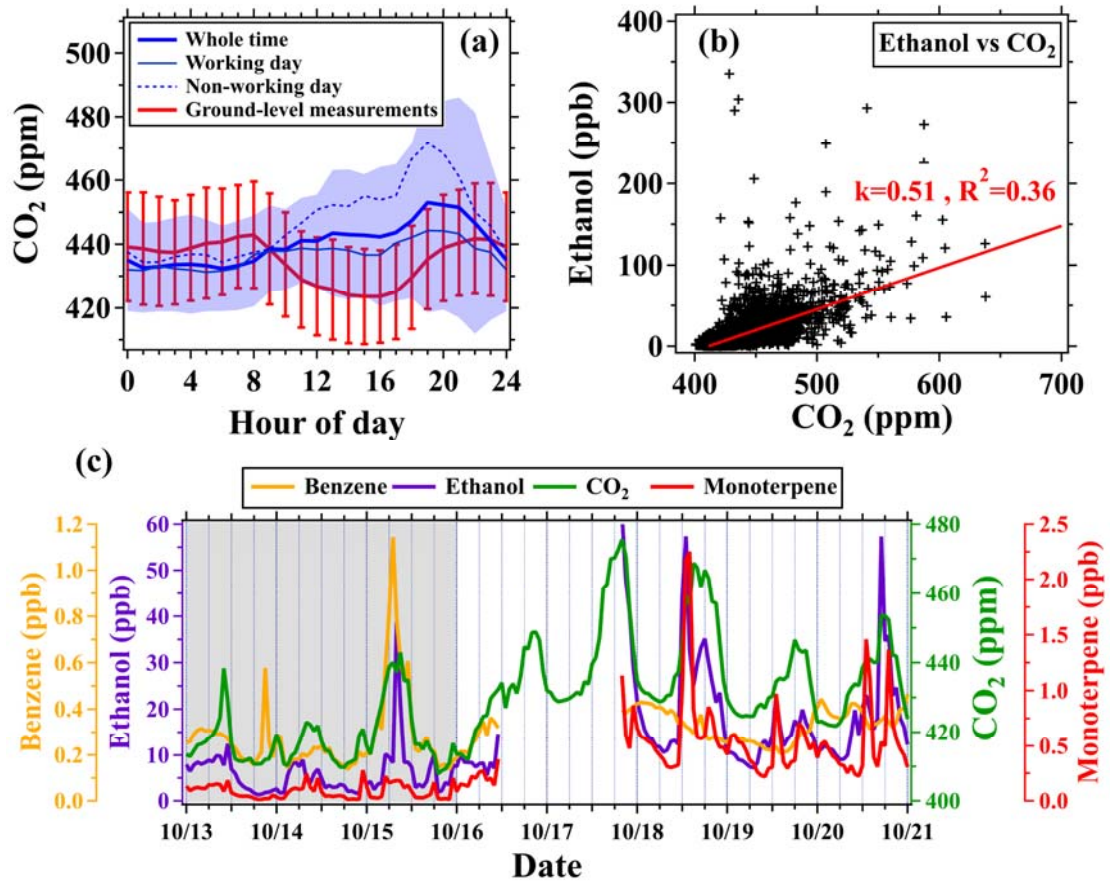
1174

1175 **Figure 3.** Diurnal variations in mixing ratios of selected VOC species measured by
 1176 PTR-ToF-MS. Thick blue solid lines and shaded areas represent averages and standard
 1177 deviations, respectively, during the CTT campaign (August 18–November 05, 2020).
 1178 Red solid lines represent averages during the GIG campaign (September 11–November
 1179 19, 2018). Thin blue solid and dashed lines represent averages in working days and
 1180 non-working (including weekends and public holidays) days, respectively, during the
 1181 CTT campaign.

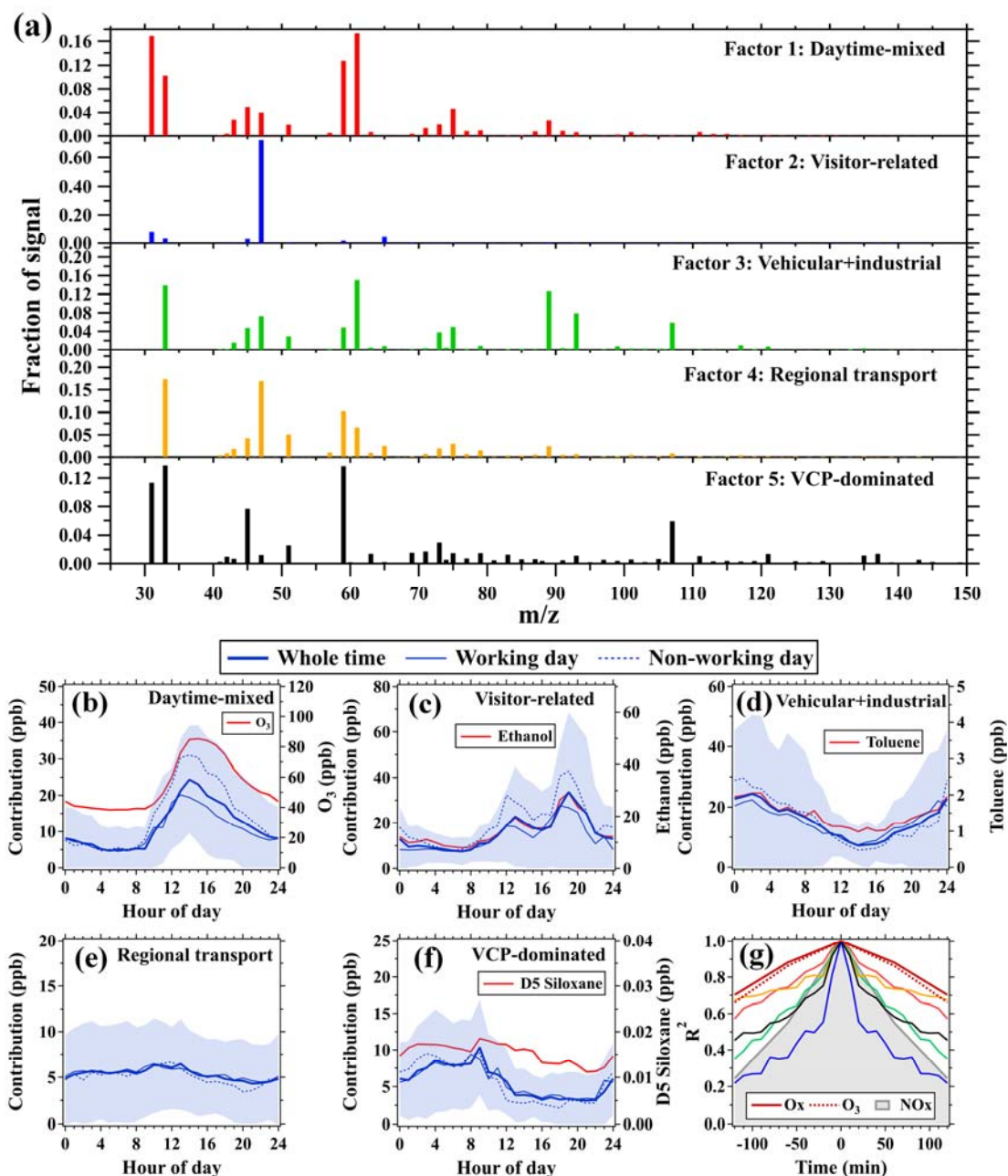


1182
 1183 **Figure 4.** (a) Diurnal profiles of ozone and NOx mixing ratios measured at the 488-m
 1184 site (mean \pm standard deviation) and the surface site (mean \pm 0.5 standard deviation)
 1185 on the CTT. (b) Autocorrelation of the time series of ozone (488 m), NOx (488 m), Ox
 1186 (488 m), and selected VOC species (450 m) during the CTT campaign. (c)
 1187 Autocorrelation of the time series of the selected VOC species at the ground level

1188 during the GIG campaign; Autocorrelation of the time series of ozone, NO_x, and O_x in
1189 panel (c) are calculated using the measurements made at the surface site of Canton
1190 Tower during the CTT campaign.



1191
 1192 **Figure 5.** (a) Diurnal variations in CO₂ mixing ratios at 450 m and the ground level,
 1193 respectively. (b) Scatterplots of 10-min mean mixing ratios of ethanol versus CO₂
 1194 mixing ratios measured at 450 m during the CTT campaign.; ~~The ground-level CO₂~~
 1195 ~~measurements were made in the GIG campaign.~~ (c) Time series of benzene, ethanol,
 1196 CO₂, and monoterpene mixing ratios measured at 450 m from October 13 to 21; The
 1197 grey shaded area indicates the period (October 13–21) when the 450-m platform was
 1198 closed due to the influence of Typhoon Kompasu.



1199

1200

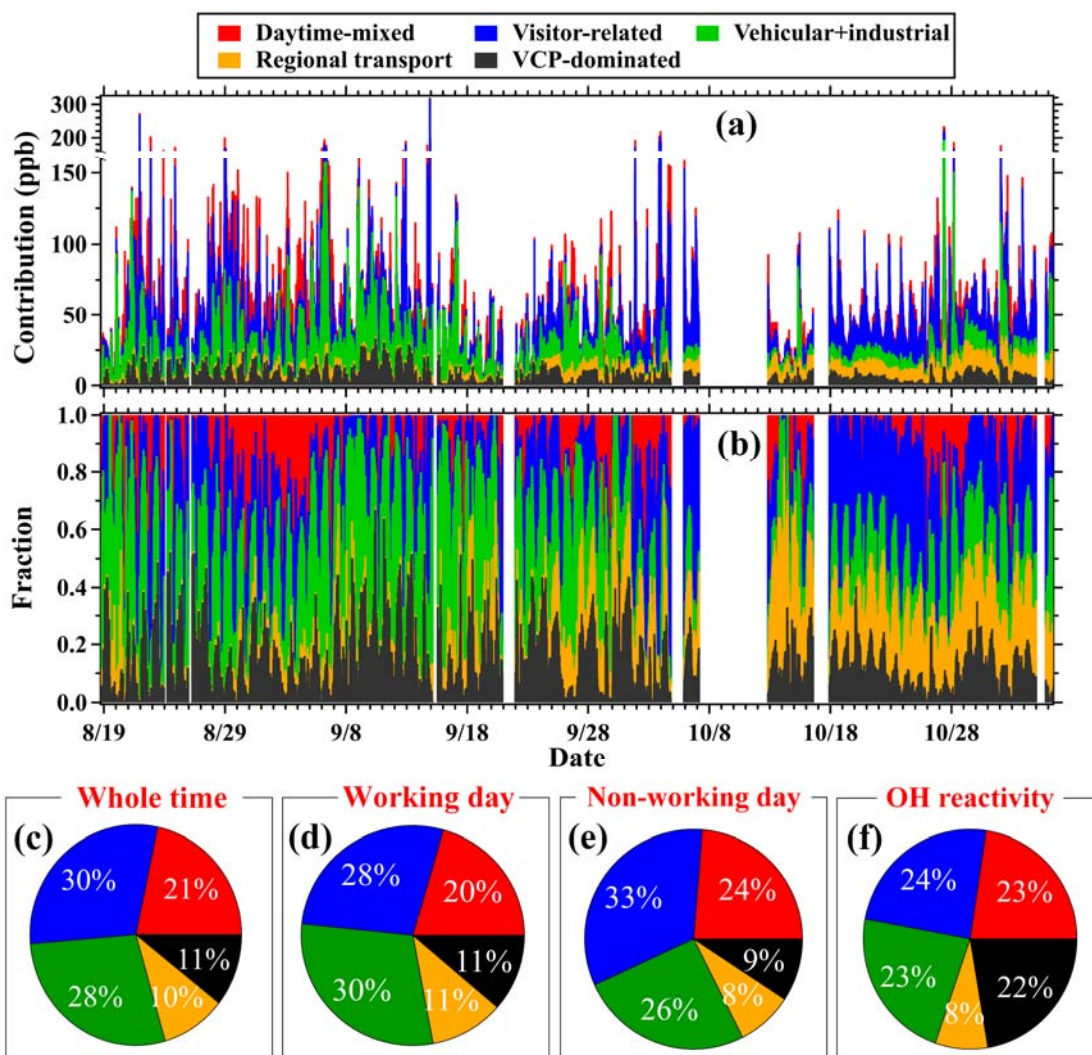
1201

1202

1203

1204

Figure 6. (a) Factor profiles ($m/z \leq 150$) of the five PMF factors; Factor profiles with a full range of the mass spectra are provided in Figure S6S7. (b-f) Average diurnal profiles of the five PMF factors and source tracers. (g) Autocorrelation of the time series of the five PMF factors along with Ox, ozone, and NOx mixing ratios at 488 m; Colors of lines are consistent with the five factors in panel (a).



1205

1206

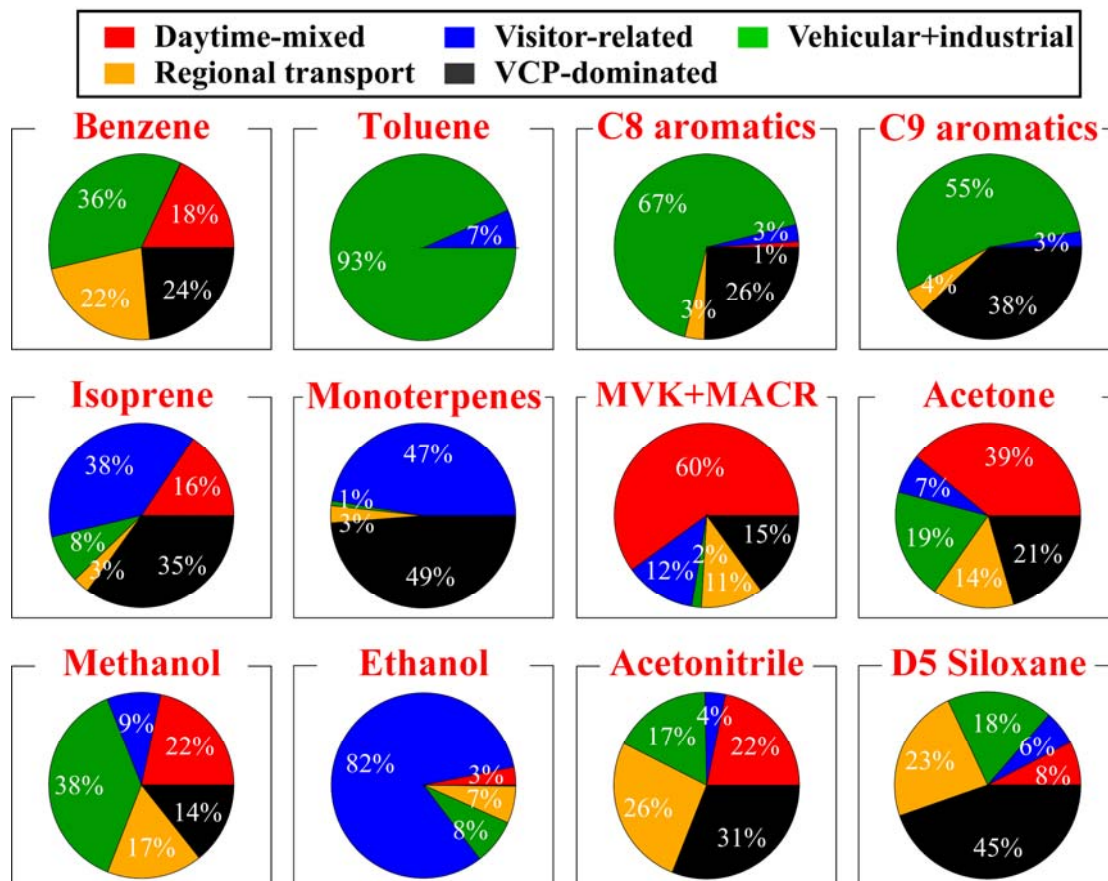
1207

1208

1209

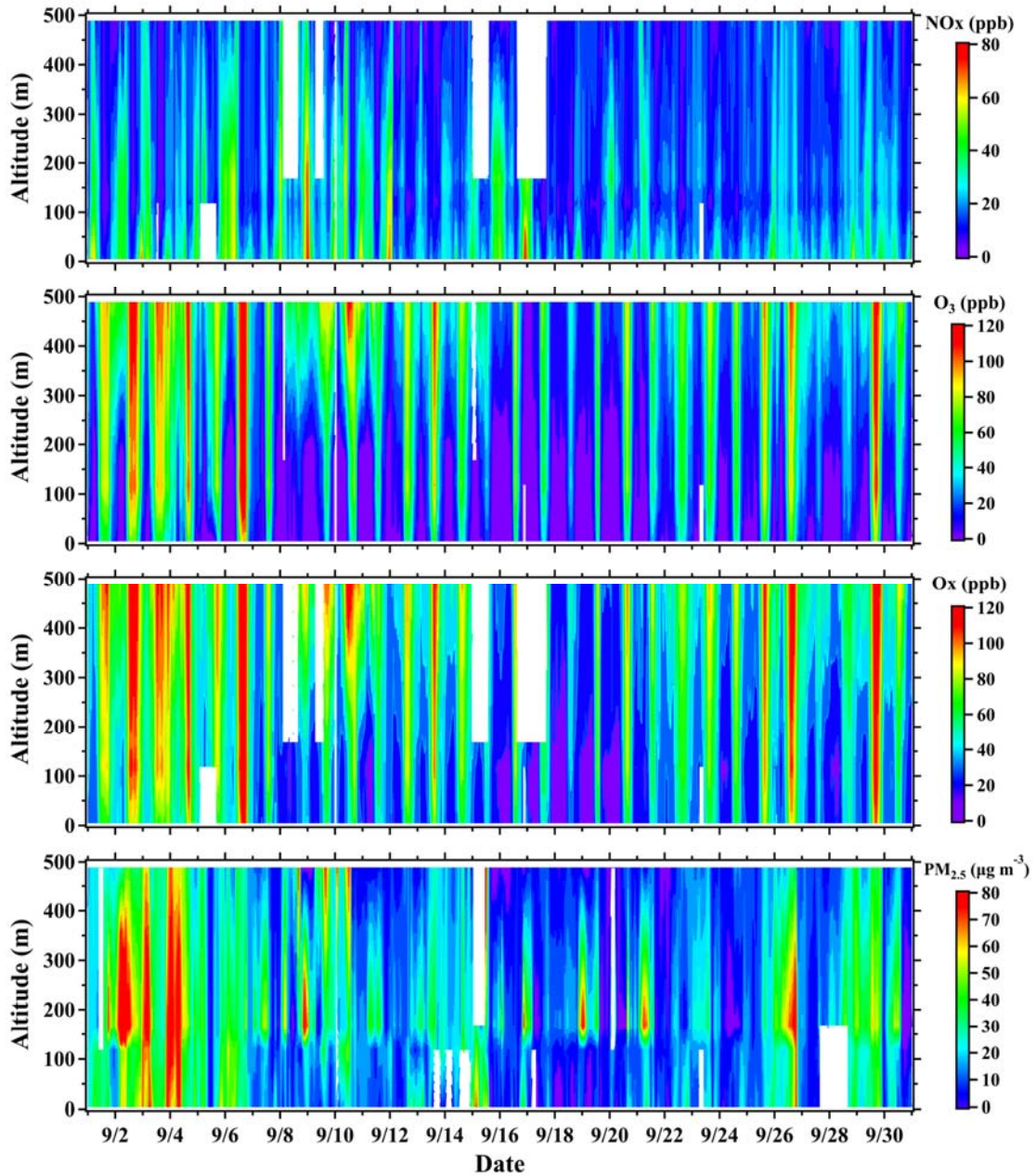
1210

Figure 7. (a-b) Stacked time series of factor fractions and factor contributions for the PMF analysis; (c-e) Average contribution percentages of the five PMF factors to (c-e) the total VOCs concentrations in the whole time, working days, and non-working days and (f) the total OH reactivities during the CTT campaign. In panel (d), only the VOCs species that have known reaction rate constants with OH radical (Table S1) were used.



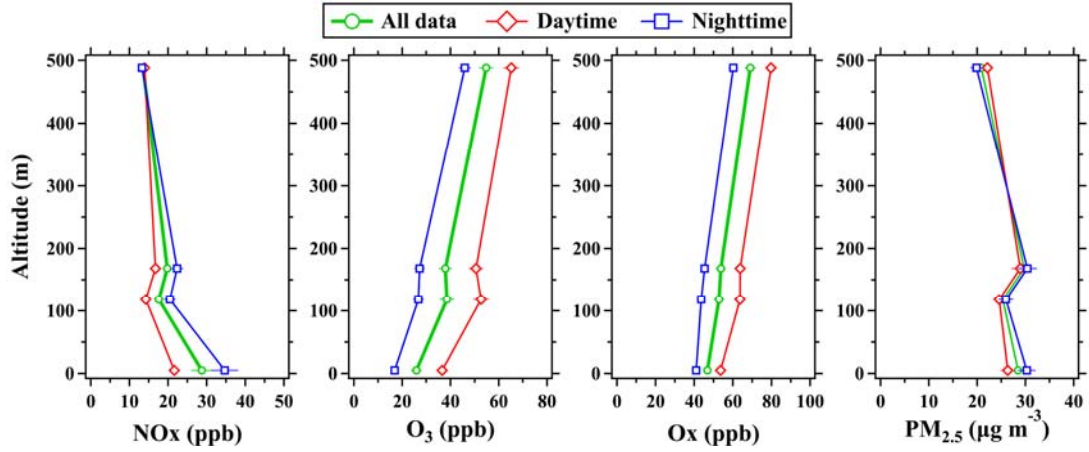
1211

1212 **Figure 8.** (a) Average contribution percentages of the five PMF factors to
 1213 concentrations of the 9 selected VOC species during the CTT campaign.



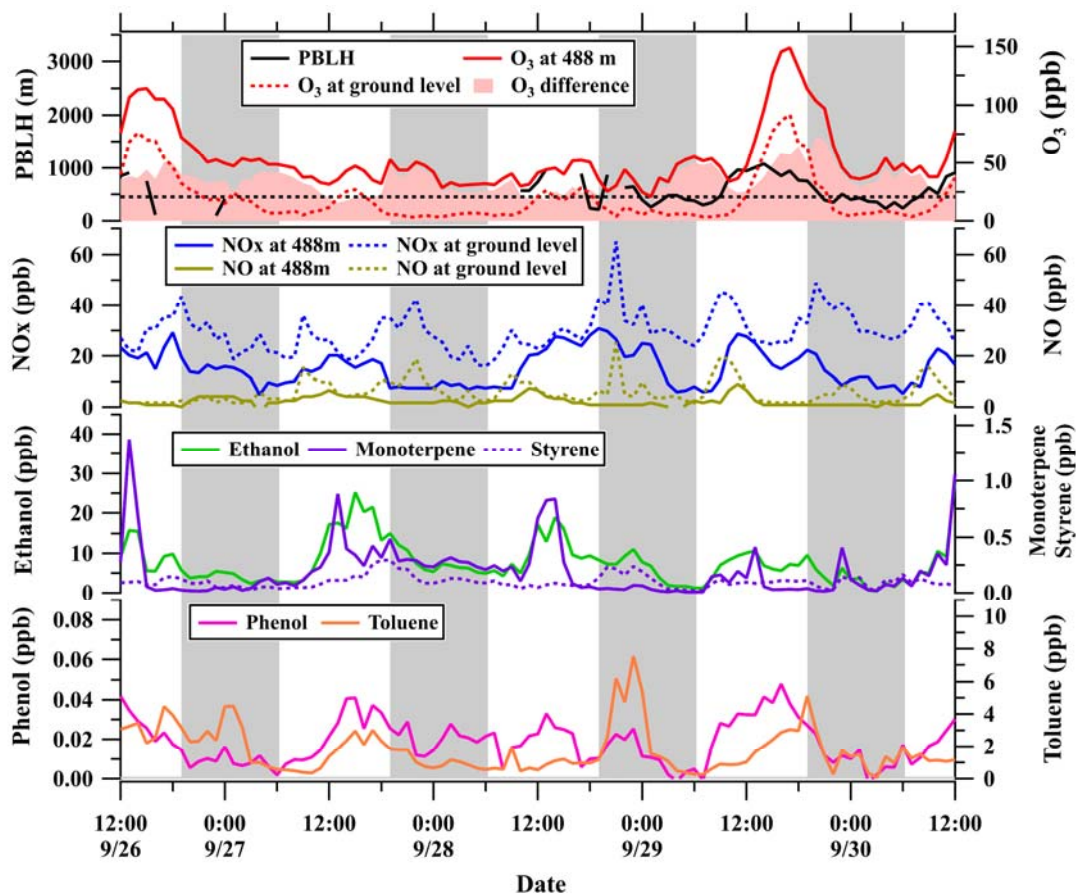
1214

1215 **Figure 9.** Time series of vertical profiles for O₃, NO_x, Ox (O₃+NO₂), and PM_{2.5}
 1216 concentrations in September during the CTT campaign. The contour plots are made
 1217 using the measurements from the four CTT sites (5 m, 118 m, 168 m, and 488 m).



1218

1219 **Figure 10.** Average vertical profiles of O₃, NO_x, Ox (O₃+NO₂), and PM_{2.5}
 1220 concentrations (mean ± 0.1 standard deviations) measured at the four CTT sites (5 m,
 1221 118 m, 168 m, 488 m) during the campaign. Daytime refers to the time between LT
 1222 08:00–18:00; nighttime refers to the time between LT 19:00–05:00.



1223

1224 **Figure 11.** Time series of O₃, NO_x, NO, ethanol, monoterpene, styrene, phenol, and
 1225 toluene mixing ratios along with planetary boundary layer height (PBLH) during
 1226 September 26–30. O₃ difference refers to the differences in ozone mixing ratios
 1227 between 488 m and 5 m. Grey shaded areas indicate nighttime periods (LT 19:00–
 1228 05:00).